Earliest Seafloor Hydrothermal Systems on Earth: Comparison with Modern Analogues

Suzanne D. Golding, Lawrence J. Duck, Elisa Young, Kim A. Baublys, Miryam Glikson, and Balz S. Kamber

Abstract Recent developments in multiple sulfur isotope analysis of sulfide and sulfate minerals provide a new tool for investigation of ore-forming processes and sources of sulfur in Archean hydrothermal systems, with important implications for the Archean sulfur cycle, the origin and impact of various microbial metabolisms and the chemistry of surface waters. In the current study we show that most of the sulfides and sulfates in the 3.49 Ga Dresser Formation and 3.24 Ga Panorama Zn–Cu field of Western Australia have non zero $\Delta^{33}S$ values that indicate variable proportions of seawater sulfate and elemental sulfur of UV-photolysis origin were incorporated into the deposits. Our results show that the multiple sulfur isotope systematics of the Dresser Formation sulfides and sulfates mainly reflect mixing between mass independently fractionated sulfur reservoirs with positive and negative $\Delta^{33}S$. Pyrite occurring with barite is depleted in ^{34}S relative to the host barite that has been interpreted as evidence for microbial sulfate reduction. We note, however, that the reported quadruple sulfur isotope systematics of pyrite-barite pairs are equally permissive of a thermochemical origin for this pyrite, which is consistent with inferred formation temperatures for the chert-barite units in excess of 100°C. The variably positive $\Delta^{33}S$ anomalies of the Panorama VHMS deposits, disequilibrium relations among sulfides and sulfates and general trend of increasing sulfide $\Delta^{33}S$ with stratigraphic height in individual ore systems most likely reflects temperature evolution and fluid mixing through the life of the hydrothermal system. The absence of sulfides with significant negative $\Delta^{33}S$ anomalies suggests that volcanic sulfur, not seawater sulfate, was the dominant sulfur source for the Panorama mineral system. The data presented here require Paleoarchean seawater to be at least locally sulfate bearing.

S.D. Golding (✉), L.J. Duck, E. Young, K.A. Baublys, and M. Glikson
School of Earth Sciences, University of Queensland, Brisbane, Queensland 4072, Australia
e-mail: s.golding1@uq.edu.au

B.S. Kamber
Department of Earth Sciences, Laurentian University, 935 Ramsey Lake Road, Sudbury, Ontario P3E 2C6, Canada

S.D. Golding and M. Glikson (eds.), *Earliest Life on Earth: Habitats, Environments and Methods of Detection*, DOI 10.1007/978-90-481-8794-2_2,

Keywords Archean sulfur cycle • Seafloor hydrothermal systems • Multiple sulfur isotopes • Thermochemical sulfate reduction • Microbial sulfate reduction • Dresser formation

1 Introduction

Submarine hydrothermal systems provide physically and chemically diverse habitats for microbial and other life and are chemically reactive environments that support abiotic synthesis of carbonaceous compounds (e.g. Kelley et al. 2005; Fiebig et al. 2007; McCollom and Seewald 2007; Proskurowksi et al. 2008). The widespread occurrence of hydrothermal systems in the early Precambrian has led to the suggestion that such environments may have constituted the cradle of life on Earth (e.g. Corliss et al. 1981; Simoneit 1995; Henley 1996; Shock 1996; Stetter 1996; Summons et al. 1996; Walter 1996; Shock and Schulte 1998; Holm and Charlou 2001; Russell 2003; Williams et al. 2005), largely because the chemistry of the H_2/CO_2 redox pair in seafloor hydrothermal systems favours the synthesis of reduced carbon compounds, the essential constituents of life (Shock 1990, 1996; Martin and Russell 2007). However, it is also generally accepted that the emergence of life in a hydrothermal vent environment would have been constrained by temperature and most likely required long lived hydrothermal activity (Poole et al. 1999; Ertem 2004; Russell et al. 2005; Russell and Hall 2006; Martin et al. 2008). As such, a low to mid temperature (≤110°C), freely convecting (non-magma driven), metalliferous seafloor hydrothermal seep or vent system like the Lost City hydrothermal field, located 30°N and some 15 km west of the Mid-Atlantic ridge (MAR) (Früh-Green et al. 2003; Kelley et al. 2005) is a most likely milieu for emergence of life on Earth (Russell et al. 2005; Russell and Hall 2006; Martin and Russell 2007; Russell 2007; Martin et al. 2008). In such environments, the serpentinisation of ophiolite complexes driven by subsurface seawater circulation, produces a self-sustaining exothermic reaction (Kelley et al. 2005), which, in the case of Lost City, has been in operation for at least 30,000 years, and may last for millions of years (Früh-Green et al. 2003; Kelley et al. 2005; Russell and Hall 2006; Martin et al. 2008). Alkaline systems such as Lost City may be representative of very early Earth (Hadean) hydrothermal environments (Kelley et al. 2005), where the eruption of Mg-rich komatiitic lavas was common (e.g. Macleod et al. 1994, and references therein). As such, these environments present as probably the most likely environment for the emergence of life given the thermodynamic and geochemical constraints imposed upon such a process (e.g. Russell et al. 2005; Russell and Hall 1997, 2006). However, the record of such ancient ophiolitic hydrothermal systems in the rock record is greatly limited; hence, the main geological focus of the search for early life is those ancient hydrothermal deposits and sedimentary sequences that have survived destruction over time.

A variety of morphological, petrological, mineralogical and geochemical approaches have been taken in the search for earliest life on Earth with recent attention focused on relatively well preserved, ca. 3.5–3.2 Ga sedimentary rocks and seafloor hydrothermal systems in the Pilbara Craton in Western Australia and the

Kaapvaal Craton in South Africa (e.g. Schopf 1993, 2006; Ueno et al. 2001, 2004, 2006; Tice and Lowe 2004; Lindsay et al. 2005; Allwood et al. 2006, 2007; Orberger et al. 2006; Westall and Southam 2006; Duck et al. 2007; Hofmann and Bolhar 2007; Glikson et al. 2008; Pinti et al. 2009). This is necessary because the oldest known sedimentary rocks circa 3.8 Ga in age, including those in Greenland in the Isua Supracrustal Belt and on Akilia Island, have experienced tectonism and high grade metamorphism, which has modified mineralogy and destroyed microstructural characteristics that might provide support for a biogenic origin of the graphite in these rocks (Fedo and Whitehouse 2002; Van Zuilen et al. 2002). While there is general agreement that life existed in the Palaeoarchean, much of the evidence is equivocal (Brasier et al. 2002, 2004, 2005; Lindsay et al. 2005), and it is possible that abiogenic carbon from Fischer-Tropsch-type synthesis (FTS) (McCollom and Seewald 2007) and/or atmospheric sources (Pavlov et al. 2001) dominated seafloor hydrothermal systems and sediments during the transition of the early Earth from geochemical to biogeochemical cycles.

In previous work we have reported the results of work on well preserved carbonaceous matter (CM) in sedimentary rocks and seafloor mineral deposits from the Warrawoona, Sulphur Springs and Gorge Creek Groups of the Pilbara Craton and the Onverwacht Group of the Kaapvaal Craton (Duck et al. 2004, 2005, 2007; Glikson et al. 2008, 2010) and multiple sulfur isotope evidence for dual sulfur sources in the 3.24 Ga Sulphur Springs massive sulfide deposit and the 3.49 Ga Dresser Formation of the Pilbara Craton (Golding and Young 2005; Golding et al. 2006). In the current study we use stable and radiogenic isotope geochemistry to understand the genesis of the hydrothermal ore deposits at Sulphur Springs and in the Dresser Formation, which are arguably and respectively the earliest well preserved and documented black smoker and epithermal style seafloor hydrothermal systems on Earth and potential habitats for early life.

2 Sulfur Isotopes in Seafloor Hydrothermal Systems and Sediments

This section provides a brief overview of our current understanding of the sulfur isotope geochemistry of seafloor hydrothermal systems and sediments and the use of multiple sulfur isotopes to constrain the early origins and activity of sulfur-based microbial life. Although the modern sulfur cycle is dominated by microbial transformations of seawater sulfate, magmatic, hydrothermal and atmospheric processes may have played a more significant role in the early Earth sulfur cycle (e.g. Canfield and Raiswell 1999; Farquhar et al. 2000; Farquhar and Wing 2003; Strauss 2003; Canfield 2005). Normal terrestrial cycling fractionates sulfur isotopes according to relative mass difference so that variations in $\delta^{33}S$ and $\delta^{36}S$ follow those in $\delta^{34}S$. The mass difference between ^{33}S and ^{32}S is about half the mass difference between ^{34}S and ^{32}S, which is why observed shifts in $\delta^{33}S$ are about half those in $\delta^{34}S$ and define the mass dependent fractionation (MDF) line ($\delta^{33}S \cong 0.515 \times \delta^{34}S$; Hulston and Thode 1965; Farquhar et al. 2000). Deviations from the mass dependent line (i.e. the $\Delta^{33}S$ record

expressed as $\Delta^{33}S = \delta^{33}S - 0.515 \times \delta^{34}S$) have been identified in many Archean rocks, as well as modern sulfate aerosols and volcanic horizons resulting from Plinean eruptions (e.g. Farquhar et al. 2000; Mojzsis et al. 2003; Ono et al. 2003; Romero and Thiemens 2003; Savarino et al. 2003). Experimental studies indicate that atmospheric gas-phase reactions (SO_2–SO photolysis) produce two main products with different mass independent fractionation (MIF), i.e., elemental sulfur aerosols with positive $\Delta^{33}S$ and sulfate aerosols with negative $\Delta^{33}S$ (Farquhar et al. 2000, 2001; Farquhar and Wing 2003; Thiemens 2006). These atmospheric sources of oxidized and reduced sulfur may be incorporated into sulfide and sulfate minerals provided the atmospheric level of oxygen is sufficiently low (i.e., $<10^{-5}$ times the present atmospheric level; Pavlov and Kasting 2002). Based on the occurrence of sulfur MIF and other geochemical proxies, the majority of researchers conclude that the early atmosphere was anoxic to neutral and evolved to an oxic atmosphere between 2.45 and 2.32 Ga (e.g. Farquhar et al. 2000, 2001, 2007; Kasting 2001; Bekker et al. 2004).

Significant mass-dependent sulfur isotope fractionation accompanies microbial utilization of sulfur, particularly sulfate reduction that is the most important process for anaerobic mineralization of organic matter in marine sediments (Ohmoto and Goldhaber 1997). This is why pyrite in modern marine sediments exhibit very negative $\delta^{34}S$ values with a fractionation of up to 70 per mil relative to modern seawater sulfate. Accordingly sulfides in the Precambrian sedimentary rock record with variable $\delta^{34}S$ values and/or a substantial fractionation relative to the sulfur isotope composition of coeval seawater sulfate have been interpreted to form by microbial sulfate reduction (e.g. Kakegawa and Ohmoto 1999; Kakegawa et al. 1999; Towe 2000; Shen et al. 2001; Habicht et al. 2002). These authors have attributed the relatively small fractionation of sulfide relative to sulfate in many Archean settings to higher rates of seawater sulfate reduction in response to limiting sulfate concentrations and/or higher temperatures. Different mass dependent sulfur isotope fractionations accompany biogeochemical processes such as sulfate and elemental sulfur reduction, disproportionation of elemental sulfur and oxidation of sulfide and elemental sulfur. Many of these transformations can also occur inorganically and result in a spectrum of fractionations between sulfide and sulfate, which is why it is not always possible to interpret the ancient sulfur isotope record unambiguously even with multiple sulfur isotopes. The three main reservoirs of biologically useful sulfur in the Archean are oceanic sulfate with positive $\delta^{34}S$ and negative $\Delta^{33}S$, elemental sulfur with positive $\Delta^{33}S$ and volcanic SO_2 and H_2S with near zero $\delta^{34}S$ and $\Delta^{33}S$ (Farquhar and Wing 2003). Thus microbial sulfate reduction produces sulfide with negative $\Delta^{33}S$, whereas sulfur reducers produce sulfide with positive $\Delta^{33}S$. Both sulfides may have similar $\delta^{34}S$ values so this distinction is only possible for pre 2.4 Ga sulfides using multiple sulfur isotopes. Significantly, virtually all sedimentary and some hydrothermal sulfides older than 2.8 Ga have positive $\Delta^{33}S$ (Fig. 1), which is inconsistent with a significant role for microbial sulfate reduction and may suggest an early origin for organisms that reduce or disproportionate elemental sulfur (Golding et al. 2006; Philippot et al. 2007). From 2.8 to 2.5 Ga, sedimentary and some hydrothermal sulfides exhibit a wide range of positive and negative $\Delta^{33}S$, which is good evidence for a sulfur cycle that included microbial sulfur and sulfate reduction (Partridge et al. 2008). On the other hand, Watanabe et al. (2009) have shown experimentally using amino acid powders and sulfate that mass independently fractionated sulfur isotopes can be

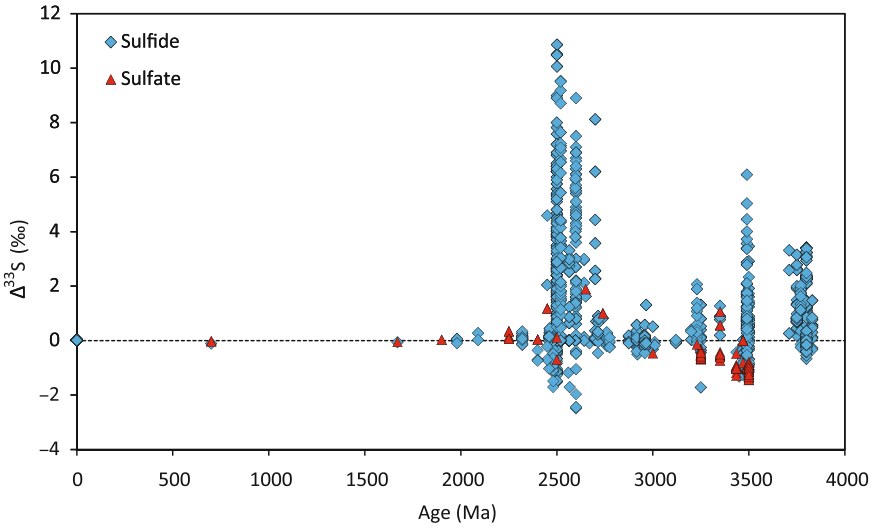

Fig. 1 A plot of $\Delta^{33}S$ versus age for sedimentary and hydrothermal sulfides and sulfates shows that the majority of sulfides older than ~2.8 Ga exhibit positive $\Delta^{33}S$ that implicates an elemental sulfur source of UV-photolysis origin irrespective of whether their precipitation occurred inorganically or was microbially mediated. Thermochemical reduction of mass dependently fractionated sulfate may also have produced small positive $\Delta^{33}S$ anomalies in some sulfides (cf. Watanabe et al. 2009). Barites and some sulfides have negative $\Delta^{33}S$ anomalies that we attribute to an ultimate seawater sulfate source. Additional data sources are Farquhar et al. (2000, 2007), Hu et al. (2003), Mojzsis et al. (2003), Ono et al. (2003, 2007, 2009), Bekker et al. (2004), Whitehouse et al. (2005), Cates and Mojzsis (2006), Ohmoto et al. (2006), Papineau and Mojzsis (2006), Bao et al. (2007), Philippot et al. (2007), Kamber and Whitehouse (2007), Kaufman et al. (2007), Partridge et al. (2008), Ueno et al. (2008) and Shen et al. (2009)

produced during thermochemical sulfate reduction at 150–200°C. The sulfur-MIF anomalies produced were relatively small but potentially complicate interpretation of multiple sulfur isotopes of ancient sedimentary rocks affected by hydrothermal alteration.

Multiple sulfur isotope studies of ancient rocks have focused on Mesoarchean and Neoarchean sedimentary successions that have been least affected by metamorphism and tectonism, particularly those in Western Australia and southern Africa (e.g. Ono et al. 2003; Bekker et al. 2004; Farquhar et al. 2007; Kaufman et al. 2007; Partridge et al. 2008). However, bedded and discordant barite deposits from Western Australia and South Africa have similar $\delta^{34}S$ values consistent with a common hydrothermal origin (Runnegar et al. 2001; Huston and Logan 2004; Bao et al. 2007), and there is wide agreement that there was a high level of hydrothermal activity in the Archean. Notwithstanding controversy as to whether the common ancestor to extant life forms was thermophilic (Doolittle 1999; Galtier et al. 1999), Archean seafloor hydrothermal environments would have supported the evolution of chemolithautotrophs and thermophiles and mesophiles that left isotopic and other biosignatures in the rock record (cf. Ueno et al. 2006). Furthermore, convective circulation of seawater is a fundamental part of seafloor hydrothermal systems, which provides a mechanism for

imparting atmospheric sulfur MIF signatures to hydrothermal sulfides whatever the process mediating their precipitation. Thus multiple sulfur isotopes in Archean seafloor hydrothermal systems and sediments provide the basis for investigation of sulfur sources, the origin and impact of various microbial metabolisms and the chemistry of surface waters, with important implications for the Archean sulfur cycle and the composition of the atmosphere. In this context, Philippot et al. (2007) undertook a multiple sulfur isotope study of different sulfide generations in the Dresser Formation of Western Australia and concluded that the negative $\delta^{34}S$ and positive $\Delta^{33}S$ of microscopic sulfides in growth zoned barite crystals provides evidence for the involvement of organisms that disproportionated elemental sulfur of atmospheric origin. More recently, Ueno et al. (2008) and Shen et al. (2009) have shown that the majority of barite-pyrite pairs in Dresser Formation barites have $\Delta^{33}S$-$\Delta^{36}S$ systematics consistent with that expected for microbial sulfate reduction.

3 Geologic Setting of Dresser Formation and Sulphur Springs Deposit

The 3.80–2.83 Ga Pilbara Craton of Western Australia (Fig. 2a) contains some of the oldest, best-preserved supracrustal rocks on Earth (Van Kranendonk 1998; Van Kranendonk et al. 2002). The craton is essentially an aggregate of granite-greenstone terranes overlain by sedimentary basins with six major elements recognized in the outcropping northern part of the craton. These are rare fragments of 3.80–3.55 Ga early crust, the 3.53–3.17 Ga East Pilbara Terrane, the 3.27–3.06 Ma West Pilbara Superterrane, the 3.20–2.89 Ga Kurrana Terrane, the 3.02–2.93 Ma De Grey Superbasin and the 2.89–2.83 Ga Split Rock Supersuite of late- to post-tectonic granitic intrusions (Van Kranendonk et al. 2004). The hydrothermal systems sampled for the present study occur within the 3.53–3.17 East Pilbara Terrane.

The Dresser Formation outcrops only in the North Pole Dome locality of the Panorama Greenstone Belt, approximately 160 km southeast of Port Hedland and 40 km west of Marble Bar (Fig. 2a). The Dresser is an upper formation of the Talga Talga Subgroup of the Warrawoona Group (Fig. 2b), which is the oldest lithostratigraphic group of the Pilbara Supergroup in the East Pilbara Terrane. It comprises a 1,000 m thick sequence of interbedded black and variously coloured chert, massive barite, minor felsic and mafic/ultramafic volcaniclastics and pillowed to massive basalts (Buick and Dunlop 1990; Nijman et al. 1999; Van Kranendonk et al. 2002, 2006b). Up to five lenticular members of bedded chert ± barite ± carbonate ± jasper, interbedded with pillow basalts have been recognized in the Dresser Formation. These stratiform units are thought to have been fed by a set of chert-barite veins that were emplaced within, and immediately above, listric normal growth faults, which were active during deposition of the cherts and carbonates (Nijman et al. 1998, 1999; Van Kranendonk 2006; Van Kranendonk et al. 2006a). The dominant lithology is extensively carbonate altered and silicified volcanics (Barley 1993), which are metamorphosed to prehnite-pumpellyite facies in the North Pole Dome area (Nijman et al. 1999; Terabayashi et al. 2003; Van Kranendonk and Pirajno 2004).

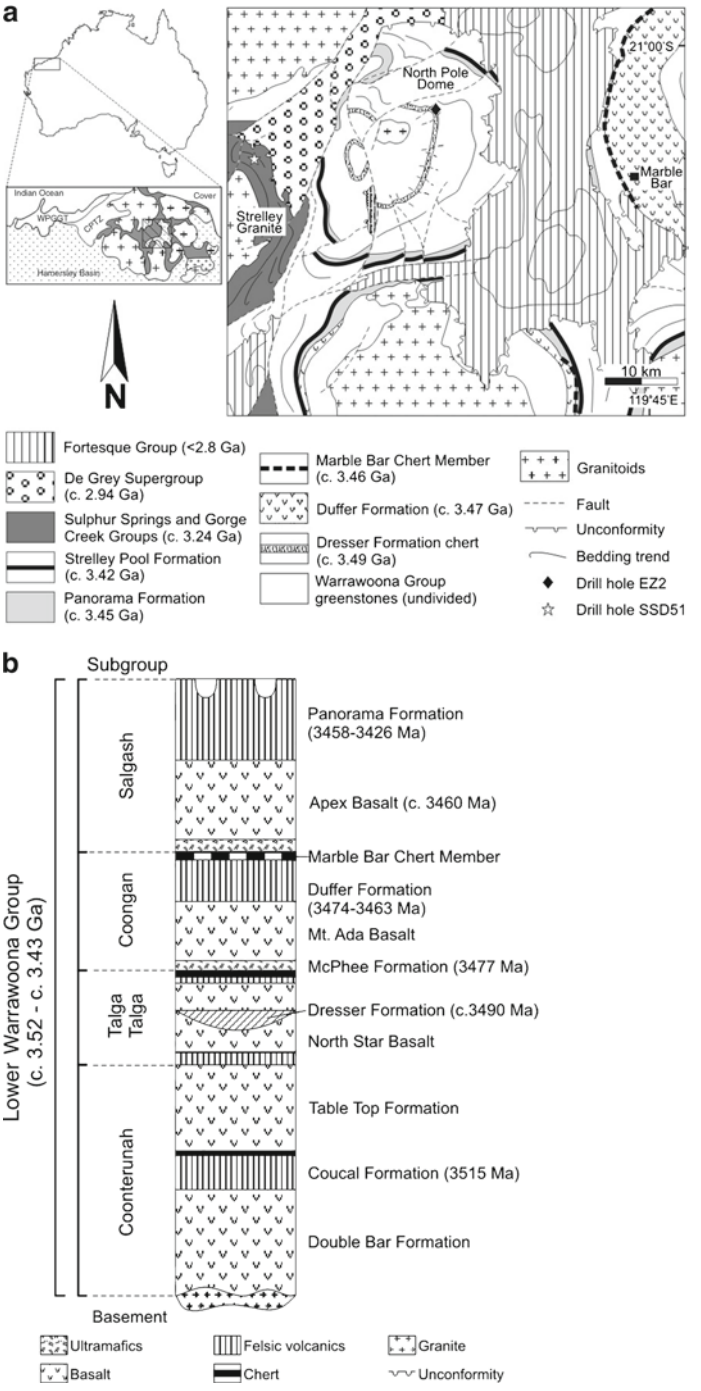

Fig. 2 (**a**) Geology of the North Pole Dome and Panorama Zn–Cu district, Pilbara Craton, (**b**) Stratigraphic column for Dresser samples

The Dresser Formation has been previously dated to circa 3,490 ± 10 Ma, using two Pb–Pb model ages for galena in presumed syngenetic barite (Thorpe et al. 1992). Recent SHRIMP U–Pb zircon dating of a felsic volcaniclastic sandstone from the top of the lowermost chert unit of the formation indicate a maximum depositional age of 3,481 ± 3.6 Ma (Van Kranendonk et al. 2008). The monzogranite exposed in the core of the North Pole Dome has been dated at 3,459 ± 18 Ma using conventional U–Pb zircon methods (Thorpe et al. 1992). New Sensitive High Resolution Ion Microprobe-Reverse Geometry (SHRIMP-RG) zircon geochronology of felsic porphyry dykes shows these intrusions have similar ages to the main granitoid body and the overlying Panorama Formation (Harris et al. 2009).

The 3.24 Ga Sulphur Springs volcanic hosted massive sulfide (VHMS) deposit is situated in the Panorama Zn–Cu field in the Soanesville Greenstone Belt, approximately 100 km southeast of Port Hedland and 50 km west of Marble Bar (Fig. 2a). The prospect was discovered in 1984 by PhD student Harry Wilhelmij, who reported finding sulfate encrustations on rocks in a then unnamed creek bed (Morant 1995). Sulphur Springs have since been described as Earth's oldest black smoker (Vearncombe et al. 1995; Morant 1998), and is interpreted to have formed at a water depth of around 1,000 m in an Archean setting equivalent to a modern back-arc basin (Vearncombe et al. 1995, 1998). A lack of any major tectonic overprint and very low metamorphic grade (prehnite-pumpellyite facies or below) has resulted in an exceptional level of structural and textural preservation (Morant 1995; Vearncombe 1995; Vearncombe et al. 1995; Duck et al. 2007).

The Sulphur Springs VHMS deposit is hosted within the upper part of the Kangaroo Caves Formation that is the upper stratigraphic unit of the 3,238–3,235 Ma Sulphur Springs Group and overlain by turbidites of the Gorge Creek Group (Morant 1995; Buick et al. 2002) (Fig. 3). The 1.5 km-thick Kangaroo Caves Formation is composed of massive, pillowed, pillow-brecciated and hyaloclastic andesitic volcanics, and dacite, rhyodacite and rhyolite sills and lavas (Brauhart 1999; Van Kranendonk 2000). VHMS mineralisation at Sulphur Springs and elsewhere in the district occurs mostly at or immediately below the marker chert, a regionally extensive silicified siltstone unit at the top of the Kangaroo Caves Formation. (Morant 1995; Vearncombe et al. 1995; Brauhart et al. 1998; Buick et al. 2002). Strata dip east such that the current exposure constitutes a cross section through a VHMS district and its underlying subvolcanic intrusion (Brauhart et al. 1998, 2000). Mineralisation consists of stratabound lenses of pyrite, sphalerite, chalcopyrite, galena, tennantite, arsenopyrite, barite, pyrrhotite and quartz, with underlying stringer zones comprising veins of quartz, pyrite, chalcopyrite, minor sphalerite and carbonate (Vearncombe et al. 1995; Barley 1998).

4 Sampling and Analytical Methods

Samples of the Dresser Formation used in this study were collected during the 2003 and 2005 field seasons from surface outcrops and diamond drill cores intersecting the massive barite deposits, which outcrop along the eastern margin of the North

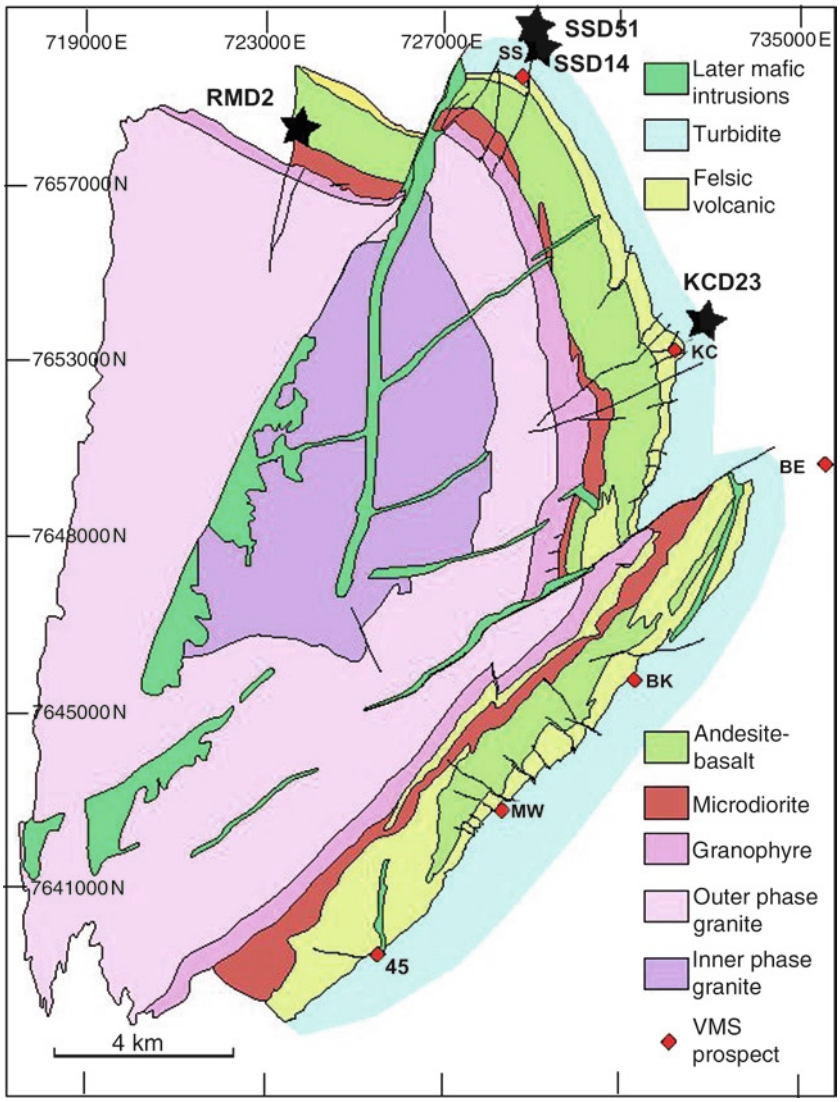

Fig. 3 Simplified local geology of the Panorama Zn–Cu district, showing locations of the VMS prospects and diamond drill holes SSD14, SSD51, RMD2 and KCD23 (adapted from Brauhart et al. 1998). The VMS prospects occur mainly at the top of the volcanic Kangaroo Caves Formation that is overlain by the turbidites of the Gorge Creek Group and intruded by the synvolcanic Strelley Granite (SS = Sulphur Springs; KC = Kangaroo Caves)

Pole Dome (Fig. 2a). The cores were drilled during the 1980s as part of the delineation of the barite deposits and are stockpiled at a location near the old Dresser mining camp (50K 753337E, 7666430N UTM), south of Panorama Homestead. Surface materials consisted primarily of massive barite, bedded chert and interbedded chert-barite samples, some of which showed obvious signs of iron-sulfide weathering.

The subsurface samples are from diamond holes EZ1 (50K 753940E, 7665686N UTM) and EZ2 (50K 753790E, 7665956N UTM) and associated core trays (Glikson et al. 2008). The drill core samples are predominantly fine-grained, carbonaceous matter (CM)-rich siliceous material variably cut by chalcedonic veins and late-stage carbonate veins. Diamond drill cores PDP2B and PDP2C from the recent Pilbara Drilling Project Provide context for interpretation of the geological setting of these samples that comprise the immediate footwall of the massive barite deposits in the case of EZ1 and EZ2 (Van Kranendonk et al. 2008).

Samples from the Sulphur Springs and Gorge Creek Groups were collected during the 2003 field season from diamond drill cores SSD14 (AMG 729043.07E, 7659869.47N), SSD51 (AMG 729103E, 7660264N) and RMD2 (AMG 723451.617E, 7658609.885N) at the Sipa Resources Port Hedland core storage facility (Fig. 3) (Duck et al. 2007). Samples of diamond drill core KCD23 also drilled by Sipa Resources Limited were subsequently obtained from the University of Western Australia Geology Museum. SSD14 commenced within the immediate hanging wall sedimentary strata of the Gorge Creek Group, intersected 4.5 m of massive sulfide mineralisation at some 220 m and a 45 m lens of combined massive sulfide and stringer zone mineralisation at some 251 m, before terminating at 354 m within the underlying felsic volcanics of the Kangaroo Caves Formation of the Sulphur Springs Group. SSD51 extends 826.2 m through the Paddy Market Formation and Corboy Formations of the Gorge Creek Group into the Kangaroo Caves Formation and intersected the marker chert horizon at some 730 m. It comprises a volcano-sedimentary sequence rich in carbonaceous cherts, ironstones and silicified shales with only minor sulfide occurrences. RMD2 was drilled in close proximity to the Strelley Granite through the lower part of the Kangaroo Caves Formation. This core comprises variably altered intermediate to mafic volcanics with lesser cherts, siltstones and arenites and is heavily intruded by dacite sills. Several semi massive sulfide horizons were intersected at some 144 m. KCD23 commenced within hanging wall turbidites of the Gorge Creek Group, intersected the marker chert and massive sulfide mineralisation between 480.6 and 504.1 m, several zones of massive to stringer sulfide mineralisation in the underlying dacite sill and terminated in dacite at 601 m.

Pyrite samples for Pb–Pb dating and sulfur isotope analysis were sourced from selected Dresser black chert samples. An attempt was made to limit the pyritic material selected to a first stage or earliest primary phase by visually isolating those areas of each selected sample not affected by cross-cut veining. Once selected, each rock sample was coarse crushed in a stainless steel percussion mortar. Sulfide-rich materials were then handpicked from the crush and transferred to 50 ml Falcon tubes prior to immersion in cold HF for a period of 48 h, with a 5 min agitation in an ultrasonic bath every 2 h. Tubes were then subjected to centrifugation to concentrate the denser pyritic material. The pyrite free supernatant fraction was decanted and the bottom residue treated with cold HCl to liberate any carbonate and fluoride complexes. The tubes again underwent centrifugation to concentrate the denser pyritic material, and the supernatant was discarded. Each sample was then thoroughly rinsed in DI water up to eight times, and the resultant pyritic slurry was dried overnight in a low temperature oven. Each sample concentrate was subsequently added

to a 250 ml conical flask of DI water and agitated to separate out the last of the carbonaceous material and concentrate the pyritic material at the base of the flask. The liquid fraction was decanted off and retained for repeat phases if needed. This filtration step was repeated until the dominant colour at the bottom of the 250 ml conical flask was that of a brassy-yellow, or until no further material remained in suspension. The pyritic fraction was then decanted into ceramic crucibles and the concentrate oven dried at 40°C. Those samples found to be of low sulfide content were repeated to increase concentration or discarded as non-usable if the final sulfide concentration was too low. Samples displaying foreign matter inclusions (e.g. barite) were hand picked clean under magnification. Macroscopic sulfide laminates and barite crystals in stratiform barite-sulfide deposits at North Pole and sulfides in Sulfur Springs samples were generally sufficiently coarse grained to be prepared by hand picking of a coarse crush or micro-drilling.

Lead isotope analyses on extracted pyrite crystals were conducted at the University of Queensland Radiogenic Isotope Laboratory (UQ-RIL). Pyrite samples were boiled in de-ionised water, then twice evaporated to dryness in open Savillex beakers using 4 ml ultra-pure HF, in order to remove any silica traces and to maximise Pb yield. Samples were then digested at 145°C for 48 h in a 1:1 HNO_3/HF mixture, converted to HBr form, and Pb separated using standard HCl–HBr chemistry, via double-pass through miniaturised anion-exchange columns. Pb-isotope ratios were acquired on a VG Sector54 instrument in static mode at pyrometer-controlled 1,350–1,450°C. Mass bias was estimated using NIST SRM 981. Corrected results are reported at 2σ confidence level (Table 1).

Table 1 Lead isotope data for Dresser pyrite samples

Sample	$^{206}Pb/^{204}Pb$	$^{207}Pb/^{204}Pb$	$^{208}Pb/^{204}Pb$	$^{207}Pb/^{206}Pb$	$^{208}Pb/^{206}Pb$	Age (Ma)	Error (±Ma)
EZ1	12.219	13.845	32.031	1.13307	2.62129	3,312	62
153.20m	±0.005	±0.006	±0.012	±0.00010	±0.00022		
EZ2a	11.803	13.573	31.699	1.15005	2.68585	3,506	53
180.50m	±0.008	±0.009	±0.022	±0.00015	±0.00032		
EZ2b	11.704	13.531	31.661	1.15245	2.69624	3,533	51
199.50m	±0.002	±0.002	±0.005	±0.00005	±0.00015		
EZ4	11.795	13.621	31.784	1.15484	2.69484	3,493	29
Core	±0.006	±0.007	±0.019	±0.00017	±0.00039		
L6-B	11.969	13.745	31.869	1.14840	2.66278	3,509	55
Surface	±0.004	±0.004	±0.011	±0.00009	±0.00020		
DF-7	11.482	13.635	31.771	1.15147	2.68291	3,567	60
Core	±0.004	±0.005	±0.013	±0.00007	±0.00019		
DF-11	11.988	13.735	31.874	1.14570	2.65880	3,508	65
Core	±0.005	±0.004	±0.010	±.00010	±0.00021		
DF-16	11.962	13.728	31.827	1.14761	2.66061	3,515	60
Core	±0.004	±0.004	±0.011	±0.00009	±0.00017		
DF-17	11.909	13.752	31.896	1.15480	2.67860	3,501	42
Core	±0.002	±0.004	±0.011	±0.00011	±0.00045		

Oxygen isotope analyses ($\delta^{18}O$) were undertaken on a Micromass 602E mass spectrometer housed at the University of Queensland Stable Isotope Geochemistry Laboratory (UQ-SIGL), which uses the dynamic gas flow method to compare unknown sample gas with reference gas. Samples comprising a minimum 20 mg of crushed, hand picked quartz were reacted overnight at 650°C with bromine pentafluoride (BrF_5) in nickel vessels in order to liberate oxygen (Clayton and Mayeda 1963). The liberated gas was converted to CO_2 by reaction with an internally heated carbon rod. Results are reported in per mil relative to the V-SMOW standard, with analytical uncertainties better than ±0.2‰ (1σ) (Table 2).

Multiple sulfur isotope analyses ($\delta^{34}S$, $\delta^{33}S$) were carried out at the UQ-SIGL using a Carlo Erba NA1500 elemental analyser coupled in continuous flow mode to an Isoprime mass spectrometer (EA-CF-IRMS) (Baublys et al. 2004). Analytical precision was determined through replicate analyses of international standards NBS127 and IAEA-S3 run as unknowns, while international standards IAEA-S1 and IAEA-S2 were used to set up the calibration for each analytical run. Results are reported in per mil relative to V-CDT and have an analytical uncertainty better than ±0.2‰ (1σ) (Tables 2 and 3).

5 Geochronology

The Pb-isotope compositions of the pyrites extracted from the samples are plotted in conventional common Pb space, i.e. $^{207}Pb/^{204}Pb$ versus $^{206}Pb/^{204}Pb$ (Fig. 4). The isotope ratio ranges for the samples from the Dresser Formation are: $^{206}Pb/^{204}Pb$ = 11.740–12.219; $^{207}Pb/^{204}Pb$ = 13.531–13.845; and $^{208}Pb/^{204}Pb$ = 31.661–32.031. The variability in isotope ratio is not random but the data define a tight linear array (Fig. 4). The slope of this array is steeper than the Geochron and implies an origin as a binary mixing line. In other words, the spread in isotope composition is not primarily caused by an age range but by a different source origin of the Pb incorporated into the pyrites, which can be successfully described with the depleted (MORB) mantle source and a global average sediment mixture (EMIX). Those samples from the EZ drill holes that plot close to the MORB curve of Kramers and Tolstikhin (1997) are interpreted to have incorporated almost pure mantle Pb (Kamber et al. 2003). In contrast, the Pb-isotope results for sample DF17 plot almost exactly onto the EMIX curve, indicating that the Pb incorporated into this sample potentially originated from the weathering/recycling of non-juvenile sediment, i.e. some older exposed continental crustal component (Green et al. 2000). The remaining Pb samples from the dataset (DF7, DF11, DF16, and L6B) have a mixed MORB/EMIX signature. For these, a 50:50 MORB-EMIX origin was used in the model age calculation.

The model age calculation was performed by fitting the $^{206}Pb/^{204}Pb$ and the $^{207}Pb/^{204}Pb$ temporal evolutions for the MORB-source mantle, the EMIX (both from Kramers and Tolstikhin 1997) and the 50:50 mixture versus time using polynomial fits. For each sample, two model ages were thus obtained by comparison of the

Table 2 Stable isotope data for Dresser sulfide, sulfate and quartz samples (WR = whole rock sample; V = vein sample)

Sample	Lithology	Sulfur species	$\delta^{34}S‰$	$\delta^{33}S‰$	$\Delta^{33}S‰$	Quartz variety	$\delta^{18}O‰$
EZ1	Black chert	Pyrite	3.47	2.07	0.29	WR	13.7
153.20m			3.65	1.98	0.11		
EZ2a	Black chert	Pyrite	2.98	1.81	0.27		
180.50m			3.07	2.81	1.24		
EZ2s	Black chert	Pyrite	2.84	1.11	−0.35		
198.20m			2.64	1.15	−0.21		
EZ2b	Black chert	Pyrite	1.83	1.75	0.81	WR	15.1
199.50m			2.55	1.00	−0.31		
			2.24	2.53	1.38		
EZ4	Black chert	Pyrite	2.49	3.19	1.91		
Core			1.17	2.05	1.45		
L6-B	Massive barite	Pyrite	−3.93	−2.90	−0.88		
Surface			−3.76	−2.83	−0.89		
		Barite	4.35	0.87	−1.37		
			4.13	0.88	−1.25		
			4.09	0.66	−1.45		
DFNP-WP38	Massive barite	Barite	4.78	1.63	−0.83		
Surface			4.64	1.13	−1.26		
			4.42	1.18	−1.09		
DFNP-WP38A	Massive barite	Barite	3.52	0.68	−1.14		
Surface			4.56	1.18	−1.16		
			4.25	1.49	−0.78		
DFNP-WP41A	Massive barite	Barite	4.80	1.51	−0.96		
Surface			4.91	1.41	−1.11		
			4.00	1.20	−0.86		
DFNP-WP45	Massive barite	Barite	4.99	1.68	−0.89		
Surface			4.68	1.39	−1.02		
			4.80	1.39	−1.08		
DF-2	Black chert	Pyrite	−8.93	−4.83	−0.22	WR	14.8
Core			−0.27	0.47	0.61		
			0.84	0.72	0.29		
			−2.45	−0.78	0.48		
DF-5	Black chert					WR	14.5
Core							
DF-7	Black chert	Pyrite	0.63	1.14	0.82		
Core			0.43	0.73	0.51		
DF-10	Black chert					WR	15.0
Core						V	14.9
DF-11	Black chert	Pyrite	1.69	1.12	0.25	WR	14.6
Core			0.95	0.20	−0.29		
			−4.31	−2.45	−0.23		
DF12	Black chert					WR	13.5
Core						V	14.6
DF-16	Black chert	Pyrite	3.93	2.81	0.79	WR	15.0
Core			4.82	2.62	0.14	V	14.8
DF-17	Black chert	Pyrite	2.28	1.53	0.36	WR	15.5
Core			1.03	1.43	0.90	V	16.1
			1.35	1.07	0.37		

Table 3 Multiple sulfur isotope data for sulfides and sulfates of the Panorama VHMS district (HW = hangingwall strata of deposit; MS = massive sulfide mineralization; FW = footwall strata of deposit)

Sample	Host lithology	Deposit	Sulfur species	$\delta^{34}S‰$	$\delta^{33}S‰$	$\Delta^{33}S‰$
SSD14-EY1	Fe-carbonate	Sulphur	Pyrite	–0.01	1.95	1.95
135.1 m	altered siltstone	Springs		0.09	2.13	2.08
		(HW)		0.27	2.29	2.15
				0.06	2.09	2.06
SSD14-EY2/1	Fe-carbonate	Sulphur	Pyrite	–0.49	0.54	0.79
147.9 m	altered siltstone	Springs		–0.28	0.71	0.85
		(HW)		–0.67	0.96	1.31
				–0.64	0.88	1.21
SSD14-EY2/2			Chalcopyrite-	1.06	0.91	1.46
147.9 m			pyrite	–0.42	1.10	1.32
				–0.62	0.91	1.23
				–0.39	1.32	1.53
				0.59	1.26	0.96
				–0.15	1.09	1.16
SSD14-EY2/3			Pyrite;	0.14	0.90	0.83
147.9 m			minor sphalerite	0.46	1.08	0.84
				–0.76	0.38	0.77
				–0.25	0.98	1.12
				0.54	1.01	0.73
SSD14-EY3	Silicified siltstone	Sulphur	Pyrite	2.44	1.66	0.40
192.3 m		Springs				
		(HW)				
SSD14-EY4	Silicified	Sulphur	Pyrite	0.78	2.44	2.03
210.6 m	volcanoclastic	Springs		0.93	2.31	1.84
		(HW)		1.01	2.33	1.80
SSD14-EY5/1	Massive sulfide	Sulphur	Chalcopyrite;	–0.49	–0.19	0.06
270.5 m		Springs	minor pyrite	–0.12	–0.02	0.04
		(MS)		–0.04	0.13	0.15
				0.58	0.51	0.21
				0.14	0.46	0.39
				0.57	0.45	0.16
SSD14-EY5/2			Pyrite; minor	–0.11	0.50	0.55
270.5 m			Chalcopyrite	0.36	0.73	0.54
				0.41	1.09	0.88
				0.30	0.23	0.18
SSD14-EY5/3			Pyrite; minor	1.64	1.24	0.40
270.5 m			Chalcopyrite	0.94	0.54	0.05
				0.69	0.56	0.21
				0.37	0.50	0.31
				0.81	0.61	0.19
				0.58	0.73	0.43
SSD14-EY5/4			Chalcopyrite;	1.20	0.91	0.30
270.5 m			minor pyrite	0.19	0.31	0.21
				0.24	0.09	–0.04

(continued)

Table 3 (continued)

Sample	Host lithology	Deposit	Sulfur species	$\delta^{34}S‰$	$\delta^{33}S‰$	$\Delta^{33}S‰$
SSD51-81/1 439.90 m	Fe-carbonate altered siltstone	Sulphur Springs (HW)	Pyrite	1.99	1.75	0.73
				2.33	1.85	0.65
				2.34	1.68	0.48
SSD51-81/2 439.90 m			Pyrite	2.44	1.76	0.51
				1.66	1.79	0.94
				2.08	1.45	0.38
				2.89	2.01	0.52
				1.81	1.31	0.37
				1.91	1.72	0.74
SSD51-102 679.15 m	Fe-carbonate altered siltstone	Sulphur Springs (HW)	Pyrite	−2.71	−0.17	1.23
				−2.09	0.35	1.42
				−2.70	−0.02	1.37
				−1.60	0.63	1.46
				−2.29	0.18	1.36
				−1.54	0.67	1.46
RMD2-01 110.1 m	Interbedded chert and Fe-carbonates	Road Master (HW)	Pyrite	1.82	1.92	0.98
				1.38	1.49	0.78
				1.50	1.76	0.98
RMD2-05 119.4 m	Fe-carbonate altered siltstone	Road Master (HW)	Pyrite	0.80	1.76	1.35
				0.47	1.28	1.04
RMD2-10 144.6 m	Chert	Road Master (MS)	Pyrite	−0.20	−0.08	0.03
				0.50	0.16	−0.10
				0.06	−0.05	−0.08
RMD2-EY1/1 149.4 m	Semi-massive sulfide	Road Master (MS)	Pyrite	0.38	0.46	0.26
				0.77	0.91	0.51
				0.60	0.40	0.10
				1.49	1.03	0.27
				0.95	0.76	0.28
RMD2-EY1/2 149.4 m			Pyrite	0.26	0.52	0.39
				0.69	0.38	0.03
				0.65	0.50	0.16
RMD2-EY1/3 149.4 m			Pyrite; minor sphalerite	1.40	0.53	−0.19
				1.21	0.79	0.17
				1.26	0.82	0.17
RMD2-12/1 151.6 m	Chert	Road Master (FW)	Vein pyrite	−0.48	−0.16	0.09
				−0.27	−0.13	0.00
				−0.62	−0.40	−0.08
RMD2-12/1 151.6 m			Vein pyrite	−0.04	0.12	0.14
				−1.18	−0.39	0.22
				−0.99	−0.18	0.33
RMD2-17/1 168.8 m	Chert	Road Master (FW)	Vein pyrite	0.13	0.30	0.23
				0.60	0.24	−0.07
				0.35	0.27	0.09
RMD2-17/1 168.8 m			Concordant pyrite	0.19	0.21	0.11
				−0.48	−0.27	−0.03
				−0.88	−0.88	−0.43

(continued)

Table 3 (continued)

Sample	Host lithology	Deposit	Sulfur species	$\delta^{34}S‰$	$\delta^{33}S‰$	$\Delta^{33}S‰$
KCD23-01 537.2 m	Silicified volcanic	Kangaroo Caves (FW)	Pyrite	2.25 2.86 2.49	1.19 1.38 1.37	0.03 –0.10 0.09
KCD23-02 546.8 m	Quartz-carbonate-pyrite-chlorite-sericite alteration	Kangaroo Caves (FW)	Pyrite	2.04 1.27 1.67 1.31 2.07	0.92 0.05 0.79 0.71 1.13	–0.13 –0.60 0.03 0.04 0.06
KCD23-05/1 556.25m	Quartz-carbonate-barite-pyrite-sericite alteration	Kangaroo Caves (FW)	Barite	6.28 6.09	3.02 3.05	–0.20 –0.08
KCD23-05/2 556.25 m			Vein pyrite	0.38 0.04 0.32	0.23 0.65 0.41	0.04 0.63 0.25
KCD23-05/3 556.25 m			Disseminated pyrite	2.38 0.48	0.52 –0.07	–0.70 –0.31

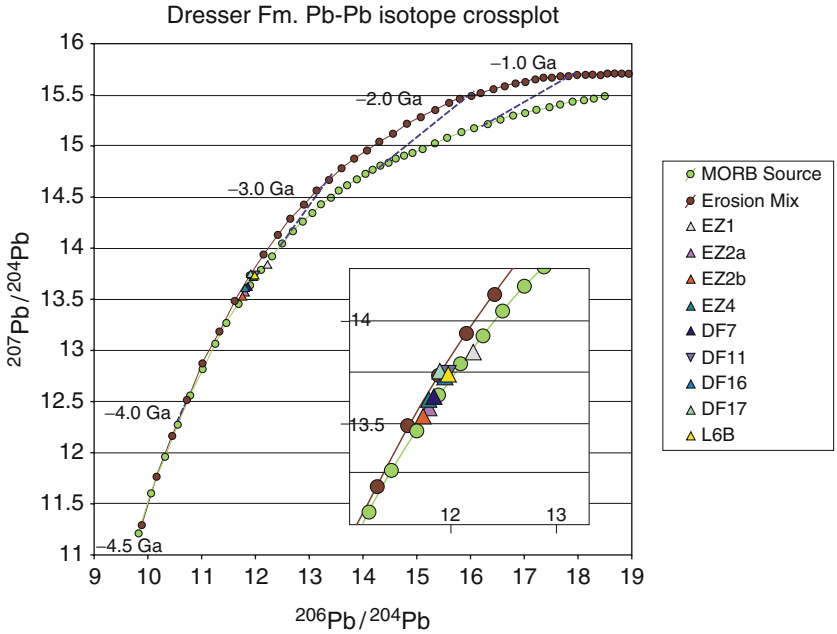

Fig. 4 Pyrite $^{207}Pb/^{204}Pb$ vs. $^{206}Pb/^{204}Pb$ of Dresser Formation pyrite plotted relative to MORB-source mantle and Erosion Mix Pb-isotope growth curves of Kramers and Tolstikhin (1997)

pyrite Pb with the appropriate model curve. The combined average of these two values per sample provided both an estimated age and error of 1σ (Table 1).

With the exception of sample EZ1 (see further below for discussion), the calculated Pb–Pb model ages (Table 1) of the sulfides extracted from the Dresser

Formation samples yield a tight cluster with an average $^{207}Pb/^{206}Pb$ age of 3,517 ± 23 Ma. Recent U–Pb SHRIMP dating of zircons isolated from a felsic tuff layer within the formation has provided a maximum depositional age of 3,481 ± 3.6 Ma respectively (Van Kranendonk et al. 2008), which is broadly consistent with the Pb–Pb model age of the stratiform barite-chert units. On the other hand, the monzogranite exposed in the core of the dome has a conventional U–Pb zircon age of 3,459 ± 18 Ma and a single porphyritic felsic intrusion has an overlapping SHRIMP-RG U–Pb zircon age of 3,438 ± 12 Ma (Harris et al. 2009). Based on these ages and local cross cutting relations between felsic porphyry dykes and quartz veins with colloform and comb textures, Harris et al. (2009) concluded that the barite-rich hydrothermal system at North Pole was related to this 3.45 Ga magmatism and contemporaneous with eruption of the overlying 3,458 ± 2 Ma Panorama Formation (Thorpe et al. 1992). Our geochronology results are not consistent with this interpretation of the timing of emplacement of the barite mineralisation in the deeper parts of the Dresser stratigraphy but do not preclude a subsequent quartz vein mineralisation overprint related to the 3.45 Ga magmatism.

The Pb–Pb model age of sample EZ1 of 3,312 ± 42 Ma is significantly younger than the rest of the sample set, and is interpreted to reflect late stage recrystallisation. Given the disparity between the calculated age of this and the other samples, EZ1 is classed as an outlier.

6 Stable Isotopes

Oxygen isotopes of vein and alteration minerals in hydrothermal systems are used to infer fluid sources and the temperature of formation of these minerals. However, processes such as fluid-rock interaction, boiling and mixing may modify the oxygen (and hydrogen) isotopic composition of the ore fluid and preclude unambiguous determination of fluid sources particularly in the absence of independent temperature estimates. The $\delta^{18}O$ values of whole rocks surrounding many ore deposits vary systematically, with low $\delta^{18}O$ values commonly associated with the most intense zones of alteration (Huston 1999). In the case of seafloor hydrothermal systems, $\delta^{18}O$ whole rock values commonly decrease with depth in the volcanic pile and in feeder zones beneath deposits, which is interpreted to reflect increasing temperature with depth and in the feeder system (Huston 1999 and references therein). However, other factors such as water/rock ratio and the $\delta^{18}O$ of the hydrothermal fluid also affect the final whole rock $\delta^{18}O$ values. Nevertheless, modelling of oxygen (and hydrogen) isotope systematics may allow distinction among these effects and provide constraints on district scale hydrology.

Sulfur isotopes are also used to determine the sources of sulfur present as sulfides and sulfates and may provide constraints on the extent of oxidation-reduction reactions in hydrothermal systems. Moreover, as discussed in Section 2, the Archean surface environment has multiple sulfur sources that have different $\delta^{34}S$ and $\Delta^{33}S$, which allows determination of whether sulfur in a hydrothermal system left the atmosphere in an oxidized or reduced form or was of magmatic origin (cf. Jamieson et al. 2006).

6.1 Dresser Formation

Oxygen isotope values were obtained for nine Dresser Formation black chert drill core samples (Table 2) to provide constraints on fluid sources and the likely depositional temperature of the chert-barite units. Originally interpreted as diagenetic replacement of evaporitic gypsum, these units are considered to be of hydrothermal origin by the majority of workers (e.g. Nijman et al. 1999; Hickman and Van Kranendonk 2004; Huston and Logan 2004; Van Kranendonk and Pirajno 2004; Van Kranendonk et al. 2008). Clean quartz chips were hand picked that allowed a distinction among whole rock and vein-sourced material for several of the samples. $\delta^{18}O$ values of the Dresser samples fall within a relatively narrow range from 13.5‰ to 16.1‰, with a mean of 14.8‰ ± 0.7‰ (n = 13). Vein quartz and black chert generally have similar $\delta^{18}O$ values (Table 2), and the results overlap the $\delta^{18}O$ values of quartz vein surface samples with epithermal textures from the North Pole Dome that range from 13.7‰ to 16.0‰ (n = 9) (Harris et al. 2009).

Two independent studies provide an indication of the possible temperature regime during deposition of the chert-barite units. Glikson et al. (2008) reported reflectance values for the various CM types identified in the black chert drill cores and obtained temperatures of 170–200°C (Ro = 1.2–1.8) and 230–240°C (Ro = 2.5–2.8) for the lowest Ro populations using the conversion of Aizawa (1990). Harris et al. (2009) undertook fluid inclusion microthermometry of quartz-chalcedony veins at various levels in the Dresser stratigraphy. These authors provided little information on the location and nature of the material analysed and appear to have focused on colloform and comb quartz including material interlayered with and overgrowing barite. The relationship between this material and the bedded cherts, barite and carbonates intersected in the Pilbara Drilling Project (Philippot et al. 2007; Van Kranendonk et al. 2008) is unclear; however, fluid inclusions in quartz have homogenization temperatures from 110–260°C, with the majority less than 210°C (Harris et al. 2009). On the other hand fluid inclusions in barite exhibited a wider range of homogenisation temperatures from 158–365°C (Harris et al. 2009), which in part may reflect post-entrapment modification. Using the quartz-water fractionation equation of Matsuhisa et al. (1979), the water in equilibrium with cherts with a mean $\delta^{18}O$ of 14.8‰ ± 0.7‰ at 150–200°C has a $\delta^{18}O$ value of −0.6‰ to 3.2‰ inconsistent with magmatic or metamorphic fluid sources (Taylor 1992).

The use of $\delta^{18}O$ values in the interpretation of fluid composition and/or palaeotemperatures from Precambrian seafloor sediments is recognised as uncertain due to the possibility that the $\delta^{18}O$ values may have been modified by isotopic reequilibration during diagenesis at elevated temperature (i.e. burial metamorphism) and postdepositional processes, such as regional metamorphism (e.g. de Ronde et al. 1997; Faure and Mensing 2005). However, the lack of a strong metamorphic overprint, as expressed by the Pb isotope results and the inferred thermal history indicators (Glikson et al. 2008) suggests these samples have not been significantly altered by any of these processes. The 2.6‰ variation in the $\delta^{18}O$ values reported in this study is most likely the result of somewhat variable hydrothermal

fluid temperatures, resulting in isotopic fractionation within the system (de Ronde et al. 1997). This interpretation allows for calculation of palaeotemperatures from the chert $\delta^{18}O$ results using a model fluid composition and a rearrangement of the Matsuhisa et al. (1979) quartz-water fractionation equation. Modelling undertaken in previous studies (e.g. de Ronde et al. 1997; Robert and Chaussidon 2006) has shown that the $\delta^{18}O$ of seawater is buffered by mid-ocean ridge hydrothermal circulation, which implies that seawater has probably had a constant $\delta^{18}0$ value of between −1.0‰ and + 1.0‰ since Archean times. Assuming a likely value of −1‰ for the Archean ocean and a seawater-dominated hydrothermal system (de Ronde et al. 1997; Muehlenbachs 1998), infers a possible depositional temperature for the Dresser Formation charts of 132–160°C. If an assumed value of −2‰ is adopted, as has been suggested (Land and Lynch 1996; Lécuyer and Allemand 1999), then temperatures would be even lower for the same samples from 123–148°C. Conversely, a +2‰ $\delta^{18}O$, equivalent to the $\delta^{18}O$ value of modern seafloor systems (Shanks et al. 1995) would give a temperature range of 166–203°C. These temperatures and the previously calculated fluid compositions are consistent with a hydrothermal origin for the chert-barite units where sea water or low latitude meteoric water was the major component of the hydrothermal system.

Multiple sulfur isotope values were obtained for fine grained sulfides separated from drill core samples of black chert, and sulfide and sulfate concentrates from outcrop samples of stratiform barite (Table 2). Our data show significant variations in $\delta^{34}S$ and $\Delta^{33}S$ among the different sulfide types. Sulfides from the black cherts exhibit a wide range of $\delta^{34}S$ values from −8.93‰ to 4.82‰ ($\delta^{34}S$ = 1.24‰ ± 2.88‰; n = 25) and positive $\Delta^{33}S$ anomalies up to 1.91‰ ($\Delta^{33}S$ = 0.45‰ ± 0.6‰; n = 25). Samples with the most positive $\Delta^{33}S$ also have positive $\delta^{34}S$ values; however, there is only a modest positive correlation between $\delta^{34}S$ and $\Delta^{33}S$ (Fig. 5). Runnegar et al. (2001) and Ueno et al. (2008) also found that disseminated pyrite in the bedded black cherts and black chert veins have positive $\Delta^{33}S$ anomalies, which they attributed to an atmospheric elemental sulfur source. The similar $\Delta^{33}S$-$\delta^{34}S$ systematics of the bedded cherts and chert veins supports a common hydrothermal origin for these units in line with field relationships (Ueno et al. 2008) although it is unclear whether the cherts are truly exhalative or formed by silicification of precursor lithologies. In this context, Philippot et al. (2007) reported that sedimentary sulfides from bedded carbonates and volcanoclastic sandstones overlying the main chert-barite unit in drill holes PDP2B and PDB2C have a limited range of $\delta^{34}S$ values (−1.4‰ ± 2.7‰) and positive $\Delta^{33}S$ anomalies of 1.0‰ ± 0.6‰. The $\delta^{34}S$ values of the black chert pyrites overlap those of the bedded carbonates rather than the volcanoclastic sandstones (Fig. 6a), which provides support for the interpretation of Van Kranendonk et al. (2008) that the barite-chert units formed at least in part by hydrothermal replacement of the bedded carbonate rocks.

The positive $\Delta^{33}S$ of sulfides analysed in the current and previous studies potentially implicates an elemental sulfur source of UV-photolysis origin, with sulfide formation occurring as a result of reduction or disproportionation of elemental sulfur (S^o) to sulfide (H_2S). The modest range of $\delta^{34}S$ values is consistent with inorganic reduction or disproportionation of elemental sulfur to sulfide or microbial

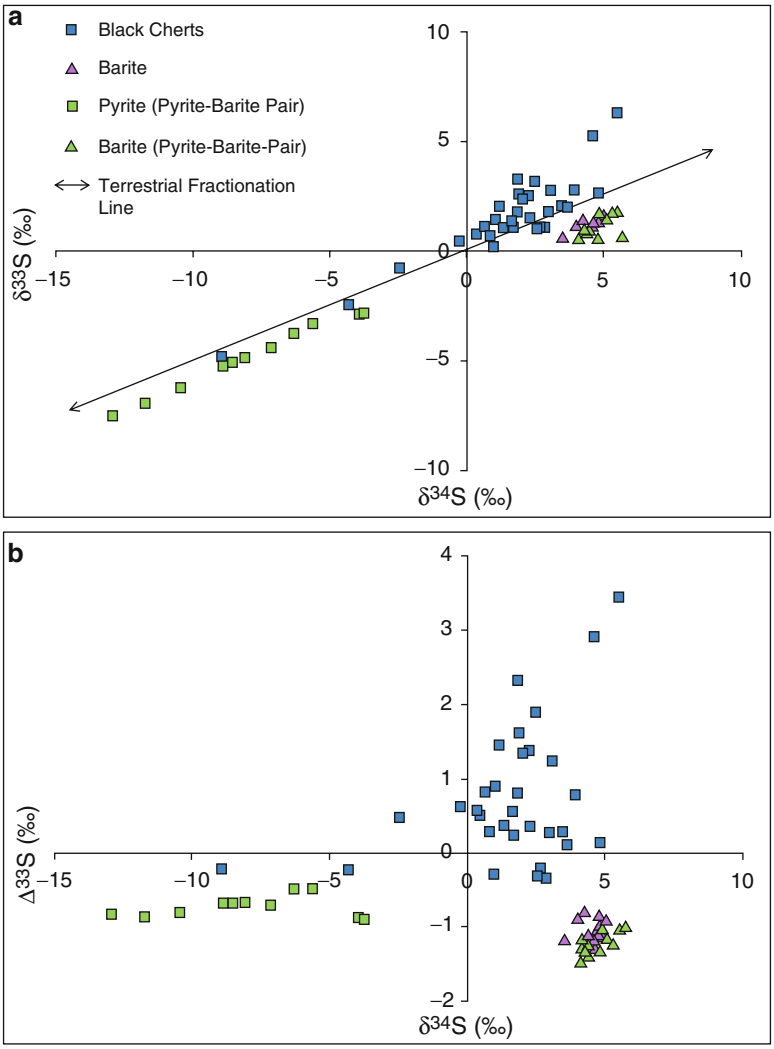

Fig. 5 (**a**, **b**) Multiple sulfur isotope compositions of sulfides and sulfates from the Dresser Formation black chert and barite units plotted with comparable data from previous work (Ueno et al. 2008; Shen et al. 2009). In this plot we have not distinguished between vein and bedded samples that have similar multiple sulfur isotope systematics

reduction of elemental sulfur to sulfide that produce ^{34}S isotope fractionations of only a few per mil (Ohmoto and Goldhaber 1997; Canfield et al. 1998; Smith 2000). The majority of black chert pyrites have positively correlated $\delta^{34}S$-$\Delta^{33}S$ values (Fig. 6a) at odds with compositions expected to result from atmospheric photolysis of volcanic gases with 193-nm UV radiation, which may reflect different atmospheric conditions (Farquhar and Wing 2003; Ono et al. 2003; Bao et al. 2007). Reactions between organic matter in the sediments and mass dependently

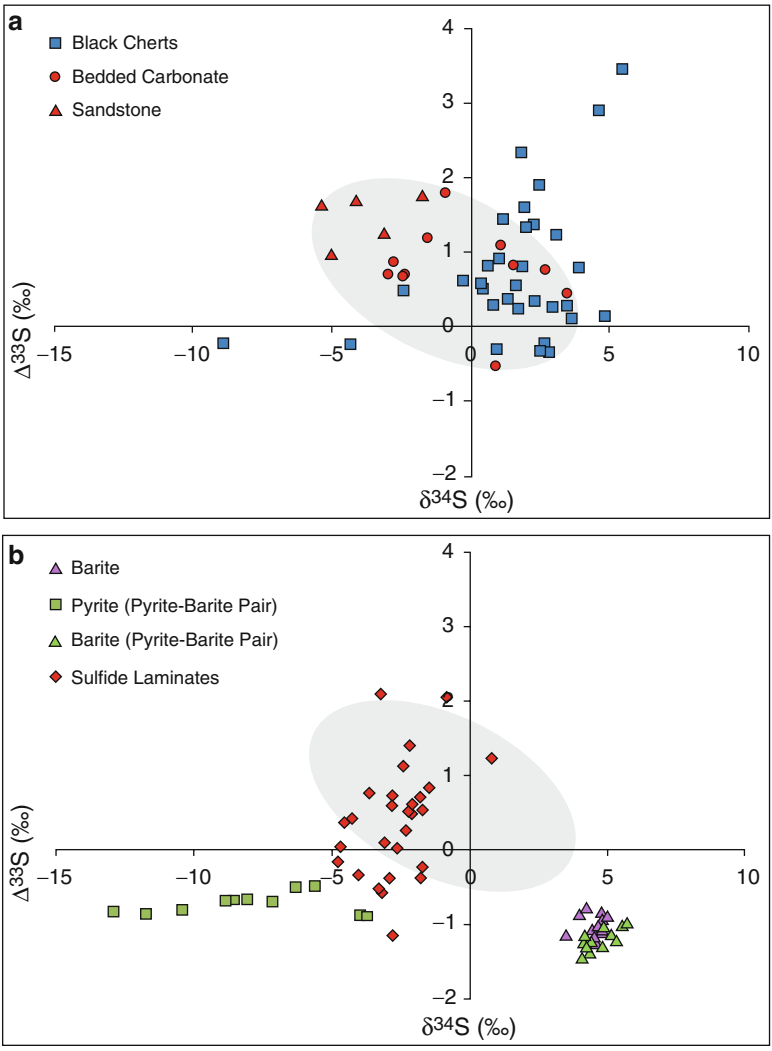

Fig. 6 (**a**) Plot of $\Delta^{33}S$ versus $\delta^{34}S$ shows that Dresser Formation black chert $\Delta^{33}S$ and $\delta^{34}S$ are positively correlated and overlap those of the bedded carbonates from drillholes PDP2B and PDP2C. Several pyrite analyses from DF2 and DF11 plot off the main trend and appear to have been mass dependently fractionated. (**b**) Plot of $\Delta^{33}S$ versus $\delta^{34}S$ shows that the macroscopic sulfide laminates from drillholes PDP2B and PDP2C have compositions intermediate between the volcanoclastic sandstones and bedded carbonates with positive $\Delta^{33}S$ anomalies (grey elliptical field) and the hydrothermal sulfides with negative $\Delta^{33}S$ anomalies. Data for drillholes PDP2B and PDP2C from Philippot et al. (2007)

fractionated sulfate-bearing hydrothermal fluids could also produce positive $\Delta^{33}S$ anomalies; however, the predominantly positive $\delta^{34}S$ values in the bedded black cherts and black chert veins militate against thermochemical sulfate reduction (TSR) that typically produces ^{34}S-depleted sulfide even in the case of the amino

acid experiments (Watanabe et al. 2009). On the other hand, several black chert pyrites have more depleted $\delta^{34}S$ values and near zero $\Delta^{33}S$ (DF 2 and DF 11; Table 2), which may suggest they were produced by thermochemical or microbial reduction of sulfate of magmatic origin.

Pyrite occurring with barite in sample L6-B has negative $\delta^{34}S$ (−3.93‰ to −3.76‰) and $\Delta^{33}S$ (−0.89‰ to −0.88‰). The L6-B barite is enriched in ^{34}S relative to the associated sulfide by some 8‰, but has a similar, albeit somewhat more negative $\Delta^{33}S$ (−1.45‰ to −1.25‰) consistent with a common sulfur source for sulfide and sulfate (Table 2). More generally the bedded barites analysed in the current study have positive $\delta^{34}S$ values of 4.46‰ ± 0.40‰ (n = 15) and negative $\Delta^{33}S$ value of −1.08‰ ± 0.20‰ (n = 15) that are similar to those found previously by Farquhar et al. (2000), Philippot et al. (2007), Ueno et al. (2008) and Shen et al. (2009) (Fig. 5). The negative $\Delta^{33}S$ anomalies in sulfates and some sulfides of the Dresser Formation are strong evidence for the incorporation of sulfate of UV-photolysis origin and at odds with the interpretation of Van Kranendonk et al. (2008) that sulfate in the Dresser Formation resulted largely from disproportionation of magmatic SO_2. Moreover, the consistency of the negative $\Delta^{33}S$ anomalies at North Pole across vein and stratiform barite indicate a common sulfur source with a significant component of MIF-sulfur. While some of the barite in the Dresser Formation may have formed by diagenetic replacement of gypsum (Shen et al. 2001, 2009), the majority of the barite shows no evidence of gypsum precursors and precipitated from solution (Runnegar et al. 2001; Van Kranendonk et al. 2008; Harris et al. 2009). Because of its highly insoluble nature, barite forms most readily when a barium-bearing reduced fluid mixes with an oxidized sulfate-bearing fluid. This is a common occurrence in Phanerozoic VHMS systems where barium-bearing hydrothermal fluids mix with sulfate-bearing seawater at and beneath the seafloor (Huston and Logan 2004). The contrasting positive and negative $\Delta^{33}S$ anomalies of the sulfide-barite and sulfide-silica veins and stratiform deposits and their cyclic formation (Van Kranendonk et al. 2008; Ueno et al 2008) suggest the Dresser barites were formed in a similar way. The interpreted occurrence of evaporites in the Dresser stratigraphy indicates that contemporaneous seawater contained sufficient sulfate at least locally to precipitate gypsum. The variations in $\Delta^{33}S$ of the pyrite laminates of Philippot et al. (2007) may also have resulted from mixing of positive and negative MIF sulfide (Fig. 6b).

Ueno et al. (2008) and Shen et al. (2009) have shown that pyrite coexisting with barite has similar or slightly higher $\Delta^{33}S$ and lower $\Delta^{36}S$ than the barite (Figs. 5b and 6b), which they interpreted in terms of microbial sulfate reduction. On the other hand, Philippot et al. (2007) identified one sulfide-barite sample with positive $\Delta^{33}S$ and negative $\delta^{34}S$ that they suggested was due to microbial sulfur disproportionation. These interpretations are consistent with the quadruple sulfur isotope systematics of the sulfide-barite pairs but take little account of the nature of the samples and the likely environment of formation. Specifically, the sulfide-barite veins both feed and crosscut the stratiform sulfide-barite units that likely formed at temperatures significantly in excess of 100°C based on fluid inclusion studies (Harris et al. 2009) and modelling of the oxygen isotopic composition of the barites (Runnegar et al. 2002). We obtained similar temperatures from modelling of the oxygen

isotopic composition of the black cherts that are spatially associated with the sulfide-barite units. These inferred temperatures preclude direct microbial involvement in the formation of the predominant sulfide in barite with negative $\Delta^{33}S$ and $\delta^{34}S$ values, which most likely formed through TSR using particulate or soluble organic matter sourced from the sediments or the hydrothermal system. Observed differences in $\Delta^{33}S$ and $\Delta^{36}S$ of the sulfide relative to coexisting sulfate can be explained by microbial sulfate reduction (Ueno et al. 2008; Shen et al. 2009) but are equally compatible with thermochemical reduction of negative MIF sulfate utilizing kerogen and/or abiogenic organic compounds (cf. Watanabe et al. 2009).

6.2 Sulphur Springs

VHMS mineralisation at Sulphur Springs and elsewhere in the Panorama Zn–Cu field occur mainly at the contact between the Sulphur Springs Group and the overlying Gorge Creek Group. The Kangaroo Caves Formation comprises basic to felsic volcanics and is intruded by the synvolcanic Strelley Granite that is interpreted to have been the heat source driving hydrothermal convection in the district (Brauhart et al. 1998, 2000). Resources have been defined at the Sulphur Springs, Kangaroo Caves and Bernts deposits (Brauhart et al. 2000) and base mineralisation interested at a number of other localities including the Roadmaster prospect. Brauhart et al. (2000) used oxygen isotopes of whole rocks to investigate fluid flow patterns and temperatures of water-rock interaction in the Panorama field. They showed there was a steady decrease in whole rock $\delta^{18}O$ values from the top to the bottom of the volcanic pile and zones of low $\delta^{18}O$ values underlying many of the VHMS deposits, which they interpreted to reflect increasing temperature with depth and in feeder zones consistent with a convective hydrothermal model. The systematically zoned alteration zones underlying Sulphur Springs and other VHMS deposits in the field record seawater-rock interaction at depth and the return of this hydrothermal fluid to the seafloor (Brauhart et al. 2000; Huston et al. 2001). A zone of sulfur depletion at the base of the volcanic pile characterised by $\delta^{34}S$ whole rock values up to 10‰ is interpreted to result from inorganic seawater sulfate reduction coupled with dissolution of volcanic sulfides (Huston et al. 2001). On the other hand sulfides from the Kangaroo Caves deposit exhibit a narrow range of $\delta^{34}S$ values around 0‰, which suggests volcanic and/or primary magmatic sulfur predominates in the VHMS deposits (Huston et al. 2001).

In the current study, multiple sulfur isotope values were obtained for sulfides microdrilled from drill core samples of hanging wall (HW) and massive sulfide mineralisation from the Sulphur Springs deposit, HW, massive sulfide and footwall (FW) mineralisation from the Roadmaster prospect and FW mineralisation from the Kangaroo Caves deposit (Table 3). Sulfides from the HW of the Sulphur Springs deposit exhibit the widest range of $\delta^{34}S$ values ($\delta^{34}S = 0.27‰ \pm 1.49‰$; n = 38) and positive $\Delta^{33}S$ anomalies up to 2.15‰ ($\Delta^{33}S = 1.16‰ \pm 0.52‰$; n = 38) (Fig. 7). Sulfides from the HW of the Roadmaster prospect exhibit a somewhat smaller range of $\delta^{34}S$ values ($\delta^{34}S = 1.19‰ \pm 0.55‰$; n = 5) and positive $\Delta^{33}S$

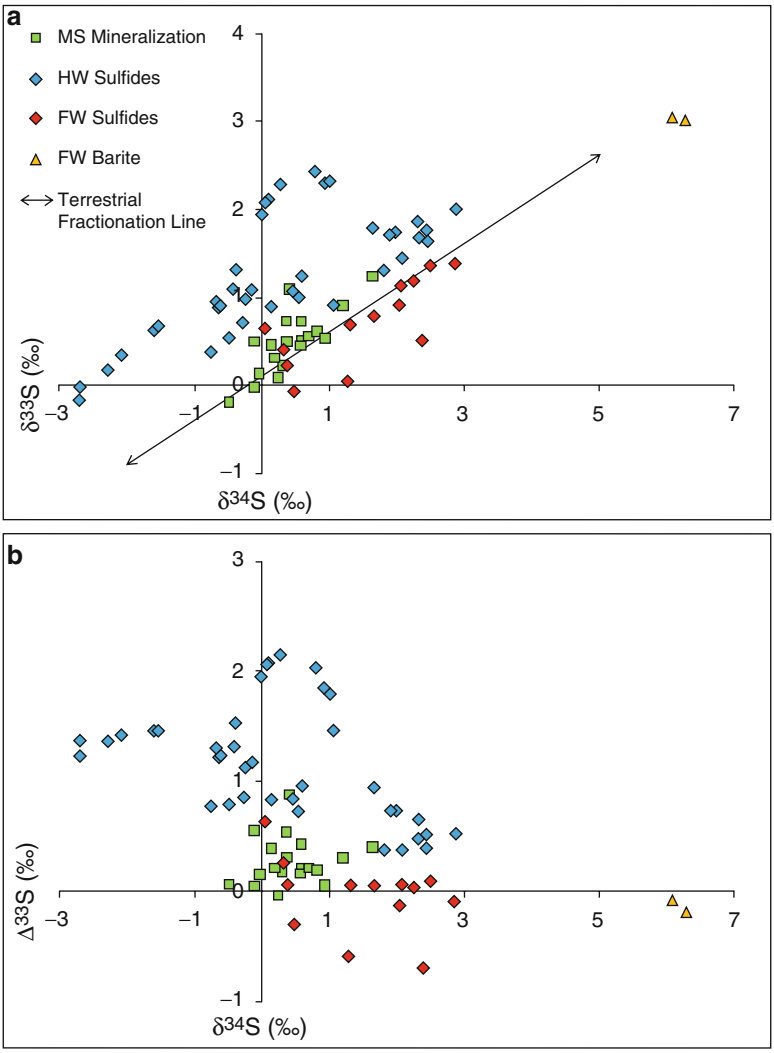

Fig. 7 (**a**, **b**) Multiple sulfur isotope compositions of sulfides and sulfates from the Sulphur Springs and Kangaroo Caves VHMS deposits separated on the basis of position within the individual ore systems that show $\Delta^{33}S$ increases with stratigraphic height (HW = hanging wall; MS = massive sulfide; FW = footwall)

anomalies up to 1.35‰ ($\Delta^{33}S$ = 1.03‰ ± 0.21‰; n = 5) (Fig. 8). HW sulfides comprise pyrite with lesser sphalerite and chalcopyrite and are preferentially hosted in Fe-carbonate altered siltstones. Siderite and ferroan carbonate is attributed to hydrothermal alteration of fine silts and organic matter rich muds of pelagic origin (Vearncombe et al. 1998), which may have provided a local elemental sulfur source of UV-photolysis origin with positive MIF.

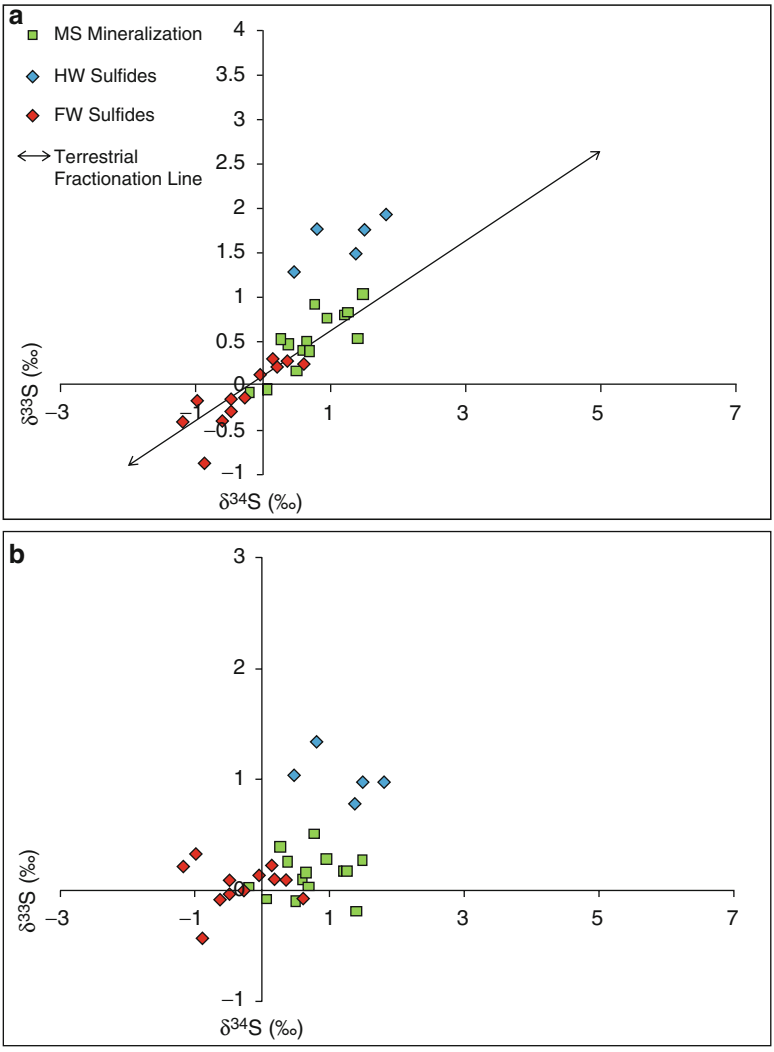

Fig. 8 (**a**, **b**) Multiple sulfur isotope compositions of sulfides from the Roadmaster prospect separated on the basis of position within the ore system that shows $\Delta^{33}S$ increases with stratigraphic height (HW = hangingwall; MS = massive sulfide; FW = footwall)

Our $\delta^{34}S$ data show a more limited range of values for massive sulfide mineralisation at Sulphur Springs ($\delta^{34}S = 0.43‰ \pm 0.50‰$; n = 19) and Roadmaster ($\delta^{34}S = 0.72‰ \pm 0.51‰$; n = 14) (Figs. 7 and 8). The $\Delta^{33}S$ data for massive sulfide mineralisation at Sulphur Springs ($\Delta^{33}S = 0.27‰ \pm 0.22‰$; n = 19) and Roadmaster ($\Delta^{33}S = 0.14‰ \pm 0.19‰$; n = 14) show mass dependent fractionation and positive $\Delta^{33}S$ anomalies in different sulfide generations of the same sample (Table 3), that indicates these sulfides had different sulfur sources and were not in isotopic equilibrium (cf. Jamieson et al. 2006). Mineral precipitation forming massive sulfide

mineralisation on the seafloor occurs primarily through mixing between hydrothermal fluid and ocean bottom water (Ohmoto et al. 1983). Sulfides in the HW volcanics likely also have isotopic compositions that reflect mixing between late stage hydrothermal fluids and connate pore waters of marine origin. In this context, the lack of variation in sulfide $\delta^{34}S$ and variably positive $\Delta^{33}S$ values of the massive sulfide mineralisation are attributed to mixing between a hydrothermal fluid dominated by MDF igneous sulfur leached from the volcanic pile and connate waters of marine origin with reduced sulfur derived from aqueous disproportionation of atmospheric elemental sulfur. HW mineralisation exhibits a wider range of sulfide $\delta^{34}S$ and more positive $\Delta^{33}S$ values that likely indicates a higher contribution of MIF sulfur from connate fluids and/or the sedimentary host rocks of the Gorge Creek Group. The lack of negative MIF sulfur in the massive sulfide and HW mineralisation is noteworthy as is the general paucity of sulfate minerals in the deposits of the Panorama field.

Barite is a minor phase in the massive sulfide mineralisation at Sulphur Springs and Kangaroo Caves and is variably overprinted by hydrothermal silica in FW stockworks. Pyrite occurring with barite in sample KCD23-05 from the FW of the Kangaroo Caves deposit has near zero $\delta^{34}S$ (0.04–2.38‰) and both small positive and negative $\Delta^{33}S$ anomalies (–0.70‰ to 0.63‰) (Table 3). The KCD23-05 barite is enriched in ^{34}S relative to pyrite by some 4–6‰ and exhibits mass dependent fractionation ($\Delta^{33}S = -0.20‰$ to $-0.08‰$). The small difference between the $\delta^{34}S$ values of the pyrite and the barite and the different $\Delta^{33}S$ values indicate that isotopic equilibrium was not attained between sulfate and sulfide during mixing of fluids and mineral precipitation. More generally our pyrite data show a modest range of $\delta^{34}S$ values for FW mineralisation at Kangaroo Caves ($\delta^{34}S = 1.50‰ \pm 0.95‰$; n = 13) and Roadmaster ($\delta^{34}S = -0.31‰ \pm 0.56‰$; n = 12) (Figs. 7 and 8). The $\delta^{34}S$ values overlap with previous data from the Kangaroo Caves deposit for pyrite ($\delta^{34}S = 0.10‰ \pm 0.625‰$; n = 8) and barite ($\delta^{34}S = 5.19‰ \pm 0.36‰$; n = 4) (Huston et al. 2001). On the other hand, FW mineralisation at the Kangaroo Caves deposit ($\Delta^{33}S = 0.27‰ \pm 0.22‰$; n = 19) and Roadmaster prospect ($\Delta^{33}S = 0.27‰ \pm 0.22‰$; n = 19) shows mass dependent fractionation and small positive and negative $\Delta^{33}S$ anomalies in different sulfide generations of the same sample (Table 3), which provides further evidence for fluid mixing and a possible component of seawater sulfate with negative sulfur MIF within the FW feeder zone. Thus there is a general trend of increasing $\Delta^{33}S$ with stratigraphic height in an individual ore system (Figs. 7 and 8); however, this zonation does not reflect absolute stratigraphic height in the district as the Sulphur Springs deposit at the top of the Kangaroo Caves Formation and the Roadmaster prospect deeper in the stratigraphy exhibit similar trends. This may suggest the hydrothermal fluid was dominated by dissolved rock sulfur of magmatic origin ($\Delta^{33}S \approx 0‰$) but included a small component of sulfur from inorganic reduction of seawater sulfate with negative $\Delta^{33}S$ (cf. Huston et al. 2001). The composition of this fluid seems to have evolved through time as disseminated pyrite with negative $\Delta^{33}S$ is overprinted by veinlet pyrite with MDF sulfur in the FW mineralisation at Roadmaster (RMD2-17) and Kangaroo Caves (KCD23-05).

7 Summary and Conclusions

Geochronology and stable isotope studies of the Dresser Formation show that the stratiform chert-barite units formed in a seafloor hydrothermal system with characteristics intermediate between a conventional seawater-dominated white smoker system and epithermal style vein mineralisation. The $\delta^{18}O$ values of the Dresser black cherts and quartz veins with epithermal textures are very similar and consistent with an intermediate temperature hydrothermal system dominated by sea water and/or low latitude meteoric water. Recent studies of modern shallow submarine hydrothermal systems have shown that active venting in water depths less than 500 m can result in epithermal style mineralisation or mineralisation transitional in character with classic massive sulfide deposits that form under deeper water conditions (e.g. Petersen et al. 2002; Sillitoe and Hedenquist 2003; Gemmell et al. 2004). In such systems black silica veins and quartz veins with epithermal textures and mineralogy indicative of near neutral hydrothermal fluids can occur with or overprint acid-sulphate style alteration as has been documented for the Dresser hydrothermal system (Van Kranendonk and Pirajno 2004; Van Kranendonk et al. 2008; Harris et al. 2009). While bedded silica-barite deposits can form directly on the seafloor at the site of shallow hot springs, solubility and kinetic considerations make it more likely that the Dresser silica-barite units were formed within unconsolidated sediments where hydrothermal fluids mixed with seawater as has been suggested for the Kuroko tetsusekiei ores of Japan (Ohmoto et al. 1983). The contrasting positive and negative $\Delta^{33}S$ anomalies of the sulfide-barite and sulfide-silica veins and stratiform deposits and their cyclic formation support this hypothesis.

Black cherts have positive $\Delta^{33}S$ values up to 1.91‰ that overlap those of a previous study (Ueno et al. 2008) and implicate an elemental sulfur source of UV-photolysis origin. The modest range of $\delta^{34}S$ values for the black cherts is consistent with inorganic reduction or disproportionation of elemental sulfur to sulfide or microbial reduction of elemental sulfur to sulfide. Reduction or disproportionation of elemental sulfur must have occurred in the hydrothermal convection cell as barite and coexisting pyrite have similar negative $\Delta^{33}S$ values suggesting a common seawater source different from that of the black chert pyrite. Atypically for Archean sulfide-sulfate pairs, the $\delta^{34}S$ values of pyrite are up to 22‰ less than that of coexisting barite and also have distinctive $\delta^{33}S/\delta^{34}S$ slopes consistent with microbial sulfate reduction (Shen et al. 2001, 2009; Ueno et al. 2008). These authors concluded on this basis that there was a strong case for the activity of sulfate reducing microbes at ca. 3.5 Ga. We note, however, that the reported quadruple sulfur isotope systematics of pyrite-barite pairs are equally permissive of a thermochemical origin for the pyrite based on the experimental work of Watanabe et al. (2009). Microbial processes were active in low temperature parts of the Dresser hydrothermal system based on the work of Glikson et al. (2008); however, the inferred temperatures of formation of the barite and associated pyrite based on fluid inclusion studies (Harris et al. 2009) and oxygen isotope modelling (Runnegar et al. 2002) are too high to permit microbial sulfate reduction and more compatible with thermochemical reduction of seawater sulfate. Moreover, the majority of sedimentary sulfides older than 2.8 Ga have positive $\Delta^{33}S$ implying an

elemental sulfur source of UV-photolysis origin and/or thermochemical reduction of mass dependently fractionated sulfate (Fig. 1), which is inconsistent with an early Archean origin for microbial sulfate reduction. Multiple sulfur isotopes are unable to distinguish microbial and inorganic sulfur reduction such that these data do not preclude an early origin for sulfur reducers.

In contrast to the controversy surrounding the Dresser Formation, Sulphur Springs and other VHMS deposits of the 3.24 Ga Panorama Zn–Cu field are similar in morphology and mineralogy to modern seafloor massive sulfide deposits albeit with somewhat different sulfur isotope systematics. Our sulfur isotope data for Sulphur Springs, Kangaroo Caves and Roadmaster are similar to other Paleoarchean VHMS deposits in that they exhibit a narrow range of $\delta^{34}S$ values in sulfides from −3‰ to 3‰, whereas Phanerozoic massive sulfide deposits range from −5‰ to 20‰ (Huston 1999; Huston et al. 2001). Barite from the Kangaroo Caves deposit is enriched in ^{34}S relative to pyrite by some 4–6‰ that is typical for Paleoarchean deposits and contrasts with Phanerozoic deposits where the difference is typically 16–22‰ (Huston 1999). The variably positive $\Delta^{33}S$ anomalies of HW, massive sulfide and FW mineralisation, disequilibrium relations among sulfides and sulfates in the same sample and general trend of increasing sulfide $\Delta^{33}S$ with stratigraphic height in individual ore systems most likely reflects temperature evolution and fluid mixing at and beneath the seafloor through the life of the hydrothermal system. In this context recent modelling of hydrothermal fluid flow in the Panorama field shows that individual deposits could have formed in some 5,000 years, whereas district scale hydrothermal activity may have lasted for >200,000 years (Schardt and Large 2009). The absence of sulfides with significant negative $\Delta^{33}S$ anomalies contrasts with late Archean VHMS deposits (Jamieson et al. 2006) and suggests that volcanic sulfur not seawater sulfate was the dominant sulfur source for the hydrothermal system.

Paleoarchean seafloor mineral systems from the Pilbara Craton of Western Australia such as the Dresser Formation and Panorama Zn–Cu field are unusual in that they contain barite, whereas barite and other sulfates are generally absent from younger Archean VHMS mineralisation (Huston and Logan 2004). Previous workers have suggested these differences may reflect temporal and/or spatial variations in seawater sulfur content and redox conditions (Eastoe et al. 1990; Huston 1999; Huston and Logan 2004). In this context the negative $\Delta^{33}S$ anomalies of barite and associated pyrite of the Dresser Formation indicate the Paleoarchean seas were at least locally sulfate bearing. The presence of negative $\Delta^{33}S$ anomalies in the shallow water Dresser Formation and their general absence in the deeper water VHMS deposits of the Panorama field may suggest the occurrence of sulfate-bearing surface waters and more anoxic bottom waters.

References

Allwood AC, Walter MR, Kamber BS et al (2006) Stromatolite reef from the Early Archaean era of Australia. Nature 441(7094):714–718

Allwood AC, Walter MR, Burch IW et al (2007) 3.43 billion-year-old stromatolite reef from the Pilbara Craton of Western Australia: ecosystem-scale insights to early life on Earth. Precambr Res 158(3–4):198–227

Aizawa J (1990) Paleotemperatures from fluid inclusions and coal rank of carbonaceous material of the Tertiary formations in northwestern Kyushu, Japan. J Jap Assoc Min Petrol Econ Geol 85:145–154

Bao HM, Rumble D, Lowe DR (2007) The five stable isotope compositions of Fig Tree barites: Implications on sulfur cycle in ca. 3.2 Ga oceans. Geochim Cosmochim Acta 71: 4868–4879

Barley ME (1993) Volcanic, sedimentary and tectonostratigraphic environments of the 3.46 Ga Warrawoona Megasequence: a review. Precambr Res 60:47–67

Barley ME (1998) Archaean volcanic-hosted massive sulphides. AGSO J Aust Geol Geophys 17:69–73

Baublys KA, Golding SD, Young E et al (2004) Simultaneous determination of $\delta^{33}S_{V\text{-}CDT}$ and $\delta^{34}S_{V\text{-}CDT}$ using masses 48, 49 and 50 on a continuous flow isotope ratio mass spectrometer. Rapid Communications in Mass Spectrometry 18:2765–2769

Bekker A, Holland HD, Wang PL et al (2004) Dating the rise of atmospheric oxygen. Nature 427:117–120

Brasier MD, Green OR, Jephcoat AP et al (2002) Questioning the evidence for Earth's oldest fossils. Nature 416:76–81

Brasier M, Green O, Lindsay J et al (2004) Earth's oldest (3.5 Ga) fossils and the 'Early Eden hypothesis': questioning the evidence. Orig Life Evol Biosph 34:257–269

Brasier MD, Green OR, Lindsay JF et al (2005) Critical testing of Earth's oldest putative fossil assemblage from the 3.5 Ga Apex chert, Chinaman Creek, Western Australia. Precambr Res 140:55–102

Brauhart CW (1999) Regional alteration systems associated with Archean volcanogenic massive sulfide deposits at Panorama, Pilbara, Western Australia. Unpublished Ph.D., Department of Geology and Geophysics, University of Western Australia, Perth

Brauhart CW, Groves DI, Morant P (1998) Regional alteration systems associated with volcanogenic massive sulfide mineralization at Panorama, Pilbara, Western Australia. Econ Geol 93:292–302

Brauhart CW, Huston DL, Andrew AS (2000) Oxygen isotope mapping in the Panorama VMS district, Pilbara Craton, Western Australia: applications to estimating temperatures of alteration and to exploration. Miner Deposita 35:727–740

Buick R, Dunlop JSR (1990) Evaporitic sediments of Early Archaean age from the Warrawoona Group, North Pole, Western Australia. Sedimentology 37:247–277

Buick R, Brauhart CW, Morant P et al (2002) Geochronology and stratigraphic relationships of the Sulphur Springs Group and Strelley granite: a temporally distinct igneous province in the Archaean Pilbara Craton, Australia. Precambr Res 114:87–120

Canfield DE (2005) The early history of atmospheric oxygen: homage to Robert M. Garrels. Annu Rev Earth Planet Sci 33:1–36

Canfield DE, Raiswell R (1999) The evolution of the sulfur cycle. Am J Sci 299:697–723

Canfield DE, Thamdrup B, Fleischer S (1998) Isotope fractionation and sulfur metabolism by pure and enrichment cultures of elemental sulfur-disproportionating bacteria. Limnol Oceanogr 43:253–264

Cates NL, Mojzsis SJ (2006) Chemical and isotopic evidence for widespread Eoarchean metasedimentary enclaves in southern West Greenland. Geochim Cosmochim Acta 70:4229–4257

Clayton RN, Mayeda TK (1963) The use of bromine pentafluoride in the extraction of oxygen from oxides and silicates for isotopic analysis. Geochim Cosmochim Acta 27:43–52

Corliss JB, Baross JA, Hofmann SE (1981) An hypothesis concerning the relationship between submarine hot springs and the origin of life on Earth. Oceanologica Acta Suppl 4:59–69

de Ronde CEJ, Channer DM, Faure K et al (1997) Fluid chemistry of Archean seafloor hydrothermal vents: implications for the composition of circa 3.2 Ga seawater. Geochim Cosmochim Acta 61:4025–4042

Doolittle WF (1999) Phylogenetic classification and the universal tree. Science 284:2124–2128

Duck LJ, Glikson M, Golding SD et al (2004) Characteristics of organic matter in sediments from the 3.24 Ga Sulphur Springs VHMS deposit, Western Australia. Geochim Cosmochim Acta Suppl 68(11S):A798

Duck LJ, Glikson M, Golding SD et al (2005) Early Archaean carbonaceous material from the Pilbara, Western Australia: its nature, characteristics and possible sources. Geochim Cosmochim Acta Suppl 69:A861

Duck LJ, Glikson M, Golding SD et al (2007) Microbial remains and other carbonaceous forms from the 3.24 Ga Sulphur Springs black smoker deposit, Western Australia. Precambr Res 154:205–220

Eastoe CJ, Compston W, Williams IS et al (1990) Sulfur isotopes in Early Proterozoic volcanogenic massive sulfide deposits: new data from Arizona and implications for ocean chemistry. Precambr Res 46:353–364

Ertem G (2004) Montmorillonite, oligonucleotides, RNA and origin of life. Orig Life Evol Biosph 34:549–570

Farquhar J, Wing BA (2003) Multiple sulfur isotopes and the evolution of the atmosphere. Earth Planet Sci Lett 213:1–13

Farquhar J, Bao H, Thiemens M (2000) Atmospheric influence of Earth's earliest sulfur cycle. Science 289:756–758

Farquhar J, Savarini J, MH AS et al (2001) Observation of wavelength-sensitive mass-independent effects during SO2 photolysis: implications for the early atmosphere. J Geophys Res 106:32829–32839

Farquhar J, Peters M, Johnston DT et al (2007) Isotopic evidence for Mesoarchaean anoxia and changing atmospheric sulphur chemistry. Nature 449:706–709

Faure G, Mensing TM (2005) Isotopes: principles and applications, 3rd edn. Wiley, New Jersey

Fedo CM, Whitehouse MJ (2002) Metasomatic origin of quartz-pyroxene rock, Akilia, Greenland, and implications for Earth's earliest life. Science 296:448–1452

Fiebig J, Woodland AB, Spangenberg J et al (2007) Natural evidence for rapid abiogenic hydrothermal generation of CH_4. Geochim Cosmochim Acta 71:3028–3039

Früh-Green GL, Kelley DD, Bernascono SM (2003) 30,000 years of hydrothermal activity at the Lost City vent field. Science 301:495–498

Galtier N, Tourasse N, Gouy M (1999) A nonhyperthermophilic common ancestor to extant life forms. Science 283:220–221

Gemmell JB, Sharpe R, Jonasson IR et al (2004) Sulfur isotope evidence for magmatic contributions to submarine and subaerial gold mineralization: conical Seamount and Ladolam Gold Deposit, Papua New Guinea. Econ Geol 99:1711–1726

Glikson M, Duck LJ, Golding SD et al (2008) Microbial remains in some Earth oldest rocks: comparison with Methanocaldococcus jannaschii, a potential analogue. Precambr Res 164:87–200

Glikson M, Hickman A, Duck LJ et al (2010) Integration of observational and analytical methodologies to characterize organic matter in early Archaean rocks: distinguishing biological from abiotically synthesized CM structures. Chapter 8, 88 to 2010

Golding, SD, Young E (2005) Multiple sulfur isotope evidence for dual sulfur sources in the 3.24 Ga Sulphur Springs deposit. Geochim Cosmochim Acta Suppl 69(10):A449

Golding SD, Young E, Duck LJ et al (2006) Multiple sulfur isotope constraints on microbial processes in Archaean seafloor environments. Geochim Cosmochim Acta Suppl 70(18):A208

Green MG, Sylvester PJ, Buick R (2000) Growth and recycling of early Archaean continental crust: geochemical evidence from the Coonterunah and Warrawoona Groups, Pilbara Craton, Australia. Tectonophysics 322:69–88

Habicht KS, Gade M, Thamdrup B et al (2002) Calibration of sulfate levels in the Archean ocean. Science 298:2372–2374

Harris AC, White NC, McPhie J et al (2009) Early Archean hot springs above epithermal veins, North Pole, Western Australia: new insights from fluid inclusion microanalysis. Econ Geol 104:793–814

Henley RW (1996) Chemical and physical context for life in terrestrial hydrothermal systems: chemical reactors for the early development of life and hydrothermal ecosystems. In: Bock GR, Goode JA (eds) Evolution of hydrothermal ecosystems on Earth (and Mars?). Wiley, New York

Hickman AH, Van Kranendonk MJ (2004) Diapiric processes in the formation of Archaean continental crust, East Pilbara granite-greenstone terrane, Australia. In: Eriksson PG,

Altermann W, Nelson DR et al (eds) The Precambrian Earth: tempos and events. Elsevier, Amsterdam/Boston; Dev Precambr Geol 12:118–139
Hofmann A, Bolhar R (2007) Carbonaceous cherts in the Barberton Greenstone Belt and their significance for the study of early life in the Archean record. Astrobiology 7:355–388
Holm NG, Charlou JL (2001) Initial indications of abiotic formation of hydrocarbons in the rainbow ultramafic hydrothermal system, Mid-Atlantic Ridge. Earth Planet Sci Lett 191:1–8
Hu G, Rumble D, Wang PL (2003) An ultraviolet laser microprobe for the in situ analysis of multisulfur isotopes and its use in measuring Archean sulfur isotope mass-independent anomalies. Geochim Cosmochim Acta 67:3101–3117
Hulston JR, Thode HG (1965) Variations in the S33, S34 and S36 contents of meteorites and their relation to chemical and nuclear effects. J Geophys Res 70:3475–3484
Huston DL (1999) Stable isotopes and their significance for understanding the genesis of volcanic-hosted massive sulfide deposits: a review. Rev Econ Geol 8:157–179
Huston DL, Logan GA (2004) Barite, BIFs and bugs: evidence for the evolution of the Earth's early hydrosphere. Earth Planet Sci Lett 220:41–55
Huston DL, Brauhart CW, Drieberg SL et al (2001) Metal leaching and inorganic sulfate reduction in volcanic-hosted massive sulfide mineral systems: evidence from the paleo-Archean panorama district, Western Australia. Geology 29:687–690
Jamieson JW, Wing BA, Hannington MD et al (2006) Evaluating isotopic equilibrium among sulfide mineral pairs in Archean ore deposits: case study from the Kidd Creek VMS deposit, Ontario, Canada. Econ Geol 101:1055–1061
Kakegawa T, Ohmoto H (1999) Sulfur isotope evidence for the origin of 3.4 to 3.1 Ga pyrite at the Princeton gold mine, Barberton Greenstone Belt, South Africa. Precambr Res 96:209–224
Kakegawa T, Kawai H, Ohmoto H (1999) Origins of pyrites in the 2.5 Ga Mt McRae Shale, the Hamersley District, Western Australia. Geochim Cosmochim Acta 62:3205–3220
Kamber BS, Whitehouse MJ (2007) Micro-scale sulphur isotope evidence for sulphur cycling in the late Archean shallow ocean. Geobiology 5:5–17
Kamber BS, Collerson KD, Moorbath S et al (2003) Inheritance of early Archaean Pb-isotope variability from long-lived Hadean protocrust. Contr Miner Petrol 145:25–46
Kasting JF (2001) The rise of atmospheric oxygen. Science 293:819–820
Kaufman AJ, Johnston DT, Farquhar J et al (2007) Late Archean biospheric oxygenation and atmospheric evolution. Science 317:1900–1903
Kelley DS, Karson JA, Früh-Green GL et al (2005) A serpentinite-hosted ecosystem: the Lost City hydrothermal field. Science 307:1428–1434
Kitajima K, Maruyama S, Utsunomiya S et al (2001) Seafloor hydrothermal alteration at an Archaean mid-ocean ridge. J Metamorph Geol 19:583–599
Kramers JD, Tolstikhin IN (1997) Two terrestrial lead isotope paradoxes, forward transport modelling, core formation and the history of the continental crust. Chem Geol 139:75–110
Krapez B (1993) Sequence stratigraphy of the Archaean supracrustal belts of the Pilbara Block, Western Australia. Precambr Res 60:1–45
Land LS, Lynch FL (1996) $\delta^{18}O$ values of mudrocks: more evidence for an ^{18}O-buffered ocean. Geochim Cosmochim Acta 60:3347–3352
Lécuyer C, Allemand P (1999) Modelling of the oxygen isotope evolution of seawater: implications for the climate interpretation of the $\delta^{18}O$ of marine sediments. Geochim Cosmochim Acta 63:351–361
Lindsay JF, Brasier MD, McLoughlin N et al (2005) The problem of deep carbon – an Archean paradox. Precambr Res 143:1–22
Macleod G, McKeown C, Hall AJ et al (1994) Hydrothermal and oceanic pH conditions at 4 Ga relevant to the origin of life. Orig Life Evol Biosph 24:19–41
Martin W, Russell MJ (2007) On the origin of biochemistry at an alkaline hydrothermal vent. Phil Trans R Soc B 362:1887–1925
Martin W, Baross J, Kelley D, Russell MJ (2008) Hydrothermal vents and the origin of life. Nat Rev Microbiol 6:805–814

Matsuhisa Y, Goldsmith JR, Clayton RN (1979) Oxygen isotope fractionation in the system quartz-albite-anorthite-water. Geochim Cosmochim Acta 43:1131–1140
McCollom TM, Seewald JS (2007) Abiotic synthesis of organic compounds in deep-sea hydrothermal environments. Chem Rev 107:382–401
Mojzsis SJ, Coath CD, Greenwood JP et al (2003) Mass-independent isotope effect in Archaean (2.5 to 3.8 Ga) sedimentary sulfides determined by ion microprobe analysis. Geochim Cosmochim Acta 67:1635–1658
Morant P (1995) The Panorama Zn–Cu VMS deposits, Western Australia. AIG Bull 16:75–84
Morant P (1998) Panorama zinc-copper deposits. In: Berkman DA, Mackenzie DH (eds) Geology of Australian and Papua New Guinean mineral deposits. The Australasian Institute of Mining and Metallurgy, Melbourne
Muehlenbachs K (1998) The oxygen isotopic composition of the oceans, sediments and the seafloor. Chem Geol 145:263–273
Nijman W, de Bruijne KCH, Valkering ME (1998) Growth fault control of Early Archaean cherts, barite mounds and chert-barite veins, North Pole dome, Eastern Pilbara, Western Australia. Precambr Res 88:25–52
Nijman W, de Bruijne KCH, Valkering ME (1999) Growth fault control of Early Archaean cherts, barite mounds and chert-barite veins, North Pole Dome, Eastern Pilbara, Western Australia (Part 2). Precambr Res 95:247–274
Ohmoto H, Goldhaber MB (1997) Sulfur and carbon isotopes. In: Barnes HL (ed) Geochemistry of hydrothermal ore deposits, 3rd edn. Wiley, New York
Ohmoto H, Mizukami M, Drummond SE et al (1983) Chemical processes of Kuroko formation. Econ Geol Mongr 5:570–604
Ohmoto H, Watanabe Y, Ikemi H et al (2006) Sulphur isotope evidence for an oxic Archaean atmosphere. Nature 442:908–911
Ono S, Eigenbrode JL, Pavlov AA et al (2003) New insights into Archaean sulfur cycle from mass-independent sulfur isotope records from the Hamersley Basin, Australia. Earth Planet Sci Lett 213:15–30
Ono S, Shanks WC III, Rouxel OJ et al (2007) S-33 constraints on the seawater sulfate contribution in modern seafloor hydrothermal vent sulfides. Geochim Cosmochim Acta 71:1170–1182
Ono S, Kaufman AJ, Farquhar J et al (2009) Lithofacies control on multiple-sulfur isotope records and Neoarchean sulfur cycles. Precambr Res 169:58–67
Orberger B, Rouchon V, Westall F et al (2006) Microfacies and origin of some Archean cherts (Pilbara, Australia). In: Reimold WU, Gibson RL (eds) Processes on the early Earth. Geol Soc Am Spec Pap 405:133–156
Papineau D, Mojzsis SJ (2006) Mass-independent fractionation of sulfur isotopes in sulfides from the pre-3770 Ma Isua Supracrustal Belt, West Greenland. Geobiology 4:227–238
Partridge MA, Golding SD, Baublys KA et al (2008) Pyrite paragenesis and multiple sulfur isotope distribution in late Archean and early Paleoproterozoic Hamersley Basin sediments. Earth Planet Sci Lett 272:41–49
Pavlov AA, Kasting JF (2002) Mass-independent fractionation of sulfur isotopes in Archaean sediments: strong evidence for an anoxic Archaean atmosphere. Astrobiology 2:27–41
Pavlov AA, Kasting JF, Eigenbrode JL et al (2001) Organic haze in Earth's early atmosphere: source of low-13C Late Archean kerogens. Geology 29:1003–1006
Petersen S, Herzig PH, Hannington MD et al (2002) Submarine gold mineralization near Lihir Island, New Ireland Fore-Arc, Papua New Guinea. Econ Geol 97:1795–1814
Philippot P, Van Zuilen M, Lepot K et al (2007) Early Archaean microorganisms preferred elemental sulfur, not sulfate. Science 317:1534–1537
Pinti DL, Mineau R, Clement V (2009) Hydrothermal alteration and microfossil artefacts of the 3,465-million-year-old Apex chert. Nat Geosci 2:640–643
Poole AM, Jeffares DC, Penny D (1999) Early evolution: prokaryotes, the new kids on the block. BioEssays 21(10):880–889
Proskurowksi G, Lilley MD, Seewald JS et al (2008) Abiogenic hydrocarbon production at Lost City hydrothermal field. Science 319:604–607

Robert F, Chaussidon M (2006) A palaeotemperature curve for the Precambrian oceans based on silicon isotopes in cherts. Nature 443:969–972
Romero AB, Thiemens MH (2003) Mass-independent sulfur isotopic composition in present-day sulfate aerosols. J Geophys Res Atmosph 108(D16):4524
Runnegar B, Dollase WA, Ketcham RA et al (2001) Early Archaean sulfates from Western Australia first formed as hydrothermal barites not gypsum evaporates. Geol Soc Am Abstr 33:A404
Runnegar B, Coath DM, Lyons JR et al. (2002) Mass-independent and mass-dependent sulfur processing through the Archean. Geochim Cosmochim Acta Suppl 66(15A):A655
Russell MJ (2003) Origin and evolution of life: clues from ore deposits. Inst Mining Metallurgy Trans Sec B Appl Earth Sci 112:177–178
Russell MJ (2007) The alkaline solution to the emergence of life: energy, entropy and early evolution. Acta Biotheor 55:133–179
Russell MJ, Hall AJ (1997) The emergence of life from iron monosulphide bubbles at a submarine hydrothermal redox and pH front. J Geol Soc Lond 154:377–402
Russell MJ, Hall AJ (2006) The onset and early evolution of life. In: Kesler SE, Ohmoto H (eds) Evolution of early Earth's atmosphere, hydrosphere, and biosphere – constraints from ore deposits. Geol Soc Am Memoir 198:1–32
Russell MJ, Hall AJ, Boyce AJ et al (2005) 100th Anniversary special paper: on hydrothermal convection systems and the emergence of life. Econ Geol 100:419–438
Savarino J, Romero A, Cole-Dai J et al (2003) UV induced mass-independent sulfur isotope fractionation in stratospheric volcanic sulfate. Geophys Res Lett 30:2131
Schardt C, Large RR (2009) New insights into the genesis of volcanic-hosted massive sulfide deposits on the seafloor from numerical modeling studies. Ore Geol Rev 35:333–351
Schopf JW (1993) Microfossils of the Early Archean apex chert: new evidence of the antiquity of life. Science 260:640–646
Schopf JW (2006) Fossil evidence of Archaean life. Phil Trans R Soc B 361:869–885
Shanks WC, Böhlke JK, Seal RR (1995) Stable isotopes in Mid-Ocean Ridge hydrothermal systems: interactions between fluids, minerals, and organisms. In: Humphris SE, Zierenberg RA, Mullineaux LS et al (eds) Seafloor hydrothermal systems: physical, chemical, biological, and geological interactions. Geophys Monogr 91:194–221
Shen Y, Buick R, Canfield DE (2001) Isotopic evidence for microbial sulfate reduction in the early Archaean era. Nature 410:77–81
Shen Y, Farquhar J, Masterson A et al (2009) Evaluating the role of microbial sulfate reduction in the early Archean using quadruple isotope systematics. Earth Planet Sci Lett 279:383–391
Shock EL (1990) Geochemical constraints on the origin of organic compounds in hydrothermal systems. Orig Life Evol Biosph 20:331–367
Shock EL (1996) Hydrothermal systems as environments for the emergence of life. In: Bock GR, Goode JA (eds) Evolution of hydrothermal ecosystems on Earth (and Mars?). Wiley, New York
Shock EL, Schulte MD (1998) Organic synthesis during fluid mixing in hydrothermal systems. J Geophys Res 103(E12):28513–28527
Sillitoe RH, Hedenquist JW (2003) Volcanotectonic settings, ore-fluid compositions and epithermal precious metal deposits. In: Simmons SF, Graham I (eds) Volcanic, geothermal, and ore-forming fluids: rulers and witnesses of processes within the Earth. Soc Econ Geol Spec Publ 10:315–343
Simoneit BRT (1995) Evidence for organic synthesis in high temperature aqueous media – facts and prognosis. Orig Life Evol Biosph 25(1–3):119–140
Smith JW (2000) Isotopic fractionation accompanying sulfur hydrolysis. Geochem J 34:95–99
Stetter KO (1996) Hyperthermophiles in the history of life. In: Bock GR, Goode JA (eds) Evolution of hydrothermal ecosystems on Earth (and Mars?). Wiley, New York
Strauss H (2003) Sulphur isotopes and the early Archaean sulfur cycle. Precambr Res 126:349–361
Summons RE, Jahnke LL, Simoneit BRT (1996) Lipid biomarkers for bacterial ecosystems: studies of cultured organisms, hydrothermal environments and ancient systems. In: Bock GR, Goode JA (eds) Evolution of hydrothermal ecosystems on Earth (and Mars?). Wiley, New York

Taylor BE (1992) Degassing of H_2O from rhyolite magma during eruption and shallow intrusion, and the isotopic composition of magmatic water in hydrothermal systems. Geol Surv Jpn Mem 279:190–195

Terabayashi M, Masadab Y, Ozawa H (2003) Archean ocean-floor metamorphism in the North Pole area, Pilbara Craton, Western Australia. Precambr Res 127:167–180

Thiemens MH (2006) History and applications of mass-independent isotope effects. Annu Rev Earth Planet Sci 34:217–262

Thorpe RI, Hickman AH, Davis DW et al (1992) Constraints to models for Archaean lead evolution from precise zircon U–Pb geochronology for the Marble Bar region, Pilbara Craton, Western Australia. In: Glover JE, Ho SE (eds) The Archaean: terrains, processes and metallogeny. Geology Department and University Extension, The University of Western Australia, Western Australia

Tice MM, Lowe DR (2004) Photosynthetic microbial mats in the 3,616-Myr-old ocean. Nature 431:549–552

Towe KM (2000) The Archaean atmosphere and sedimentary sulfides. Science 289:1297

Ueno Y, Isozaki Y, Yurimoto H et al (2001) Carbon isotopic signatures of individual Archean microfossils (?) from Western Australia. Int Geol Rev 43:196–212

Ueno Y, Yoshioka H, Maruyama SY et al (2004) Carbon isotopes and petrography of kerogens in 3.5-Ga hydrothermal dikes in the North Pole area, Western Australia. Geochim Cosmochim Acta 68:573–589

Ueno Y, Yamada K, Yoshida N et al (2006) Evidence from fluid inclusions for microbial methanogenesis in the early Archaean. Nature 440:516–519

Ueno Y, Ono S, Rumble D et al (2008) Quadruple sulfur isotope analysis of ca. 3.5 Ga Dresser formation: new evidence for microbial sulfate reduction in the early Archean. Geochim Cosmochim Acta 72:5675–5691

Van Kranendonk MJ (1998) Litho-tectonic and structural components of the North Shaw 1:100000 sheet, Archaean Pilbara Craton. In: 1997–98 Annual Review, Geological Survey of Western Australia

Van Kranendonk MJ (2006) Volcanic degassing, hydrothermal circulation and the flourishing of early life on Earth: a review of the evidence from c. 3490–3240 Ma rocks of the Pilbara Supergroup, Pilbara Craton, Western Australia. Earth Sci Rev 74:197–240

Van Kranendonk MJ, Pirajno F (2004) Geochemistry of metabasalts and hydrothermal alteration zones associated with c. 3.45 Ga chert and barite deposits: implications for the geological setting of the Warrawoona Group, Pilbara Craton, Australia. Geochem Explor Environ Anal 4:253–278

Van Kranendonk MJ, Hickman AH, Smithies RH et al (2002) Geology and tectonic evolution of the Archean North Pilbara Terrain, Pilbara Craton, Western Australia. Econ Geol 97:695–732

Van Kranendonk MJ, Smithies RH, Hickman AH et al (2004) Event stratigraphy applied to 700 million years of Archaean crustal evolution, Pilbara Craton, Western Australia. In: 2003–04 Annual Review. Geological Survey of Western Australia

Van Kranendonk MJ, Hickman AH, Huston DL (2006a) Geology and mineralization of the east Pilbara – a field guide. Western Australia Geological Survey, Record 2006/16

Van Kranendonk MJ, Hickman AH, Smithies RH et al (2006b) Revised lithostratigraphy of Archean supracrustal and intrusive rocks in the northern Pilbara Craton, Western Australia. Western Australia Geological Survey, Record 2006/15

Van Kranendonk MJ, Philippot P, Lepot K et al (2008) Geological setting of Earth's oldest fossils in the ca. 3.5 Ga Dresser Formation, Pilbara Craton, Western Australia. Precambr Res 167:93–124

van Zuilen MA, Lepland A, Arrhenius G (2002) Reassessing the evidence for the earliest traces of life. Nature 418:627–630

Vearncombe S (1995) Volcanogenic massive sulphide-sulphate mineralisation at Strelley, Pilbara Craton, Western Australia. Unpublished PhD, Department of Geology and Geophysics, University of Western Australia, Perth

Vearncombe S, Barley ME, Groves DI et al (1995) 3.26 Ga black smoker-type mineralization in the Strelley Belt, Pilbara Craton, Western Australia. J Geol Soc Lond 152:587–590

Vearncombe S, Vearncombe JR, Barley ME (1998) Fault and stratigraphic controls on volcanogenic massive sulphide deposits in the Strelley Belt, Pilbara Craton, Western Australia. Precambr Res 88:67–82

Walter MR (1996) Ancient hydrothermal ecosystems on Earth: a new palaeobiological frontier. In: Bock GR, Goode JA (eds) Evolution of hydrothermal ecosystems on Earth (and Mars?). Wiley, New York

Watanabe Y, Farquhar J, Ohmoto H (2009) Anomalous fractionations of sulfur isotopes during thermochemical sulfate reduction. Science 324:370–373

Westall F, Southam G (2006) The early record of life. In: Benn K, Marescha J-C, Condie KC (eds) Archean geodynamics and environments. American Geophysical Union, Washington, DC; Geophys Monogr Ser 164:283–304

Whitehouse MJ, Kamber BS, Fedo CM et al (2005) Integrated Pb- and S-isotope investigation of sulphide minerals from the early Archaean of southwest Greenland. Chem Geol 222:112–131

Williams LB, Canfield B, Voglesonger KM et al (2005) Organic molecules formed in a “primordial womb”. Geology 33:913–916

http://www.springer.com/978-90-481-8793-5

Earliest Life on Earth: Habitats, Environments and Methods of Detection

Golding, S.D.; Glikson, M. (Eds.)
2011, XVI, 316 p., Hardcover
ISBN: 978-90-481-8793-5